KERNFORSCHUNGSZENTRUM

KARLSRUHE

September 1966

KFK 482

Institut für Neutronenphysik und Reaktortechnik

Evaluation of Reactor Physics Experiments on the Coupled Fast-Thermal Argonaut Reactor Stark

I. Barleon, A. Bayer, Chr. Brückner, K. Burkart, G. Fieg, D. Kuhn, J. Kußmaul, H. Meister, H. Seufert, D. Stegemann, H. Werle

GESELLSCHAFT FÜR KERNFORSCHUNG M. B. H.

KARLSRUHE

KERNFORSCHUNGSZENTRUM KARLSRUHE

September 1966 KFK 482

Institut für Neutronenphysik und Reaktortechnik

EVALUATION OF REACTOR PHYSICS EXPERIMENTS ON THE COUPLED FAST-THERMAL ARGONAUT REACTOR STARK *

L.Barleon, A.Bayer, Chr.Brückner, K.Burkart, G.Fieg, D.Kuhn, G.Kußmaul, H.Meister, H.Seufert, D.Stegemann, H.Werle

Paper presented at the International Conference on Fast Critical Experiments and their Analysis held at Argonne (Illinois), Oct. 10-13, 1966

* Work performed within the association in the field of fast reactors between the European Atomic Energy Community and Gesellschaft für Kernforschung m.b.H., Karlsruhe

EVALUATION OF REACTOR PHYSICS EXPERIMENTS ON THE COUPLED FAST-THERMAL ARGONAUT REACTOR STARK

L.Barleon, A.Bayer, Chr.Brückner, K.Burkart, G.Fieg, D.Kuhn, G.Kussmaul, H.Meister, H.Seufert, D.Stegemann, and H.Werle

Abstract

STARK is a coupled zero-power reactor consisting of a subcritical fast core driven by a surrounding light-water moderated thermal zone. Four different fast core loadings, containing up to 107 kg ^{235}U, have been investigated so far, one of them with a CH_2 - admixture to simulate the spectrum of a steam-cooled reactor.

A number of experiments have been performed to obtain information on the neutron spectrum in the fast zone: spatial distributions of reaction rates were determined by fission chamber and foil techniques, differential neutron spectra were studied by proton-recoil proportional counters, and reactivity worths of samples were measured in the fast core with a square-wave pile oscillator. Also integral parameters of the entire system were obtained by various kinetic methods.

The experimental results are compared with one-dimensional diffusion and S_4-calculations using the Russian 26-group cross-section set. The experimental data give no indication of larger deviations from the calculated spectra in the kev- and Mev-region, whereas discrepancies were found in the lower ev-region. The integral reactor parameters (neutron lifetime, critical mass, partition of reactor power between the zones) were found to agree reasonably well with the calculation.

1. Introduction

The zero-power facility STARK is a flexible fast-thermal reactor consisting of a subcritical fast core and a surrounding Argonaut-type thermal driver zone. The basic concept of the system [1] dates back to 1962 when it was recognized that a flexible source reactor would be needed in the earlier stages of the Karlsruhe fast reactor program and, therefore, it was decided to convert the Argonaut-Reactor at Karlsruhe into a coupled fast-thermal assembly. Compared to the ZPR V experiments [2], only moderate fast-core power contributions ($\lesssim 0.40$) were planned such that the safety characteristics of the reactor still correspond to those of an all-thermal system.

Since the operation of STARK began in 1964, a number of reactor physics experiments have been completed. The experimental program was aimed at two main points:

(a) development of experimental techniques for investigating fast zero-power systems, especially fast reactor mock-ups on the critical assembly SNEAK [3],

(b) investigation of the reactor physics properties of the coupled system STARK and comparison of experimental data with multigroup calculations.

The present paper primarily deals with the second point of this program, whereas the first point is partly treated in [4].

Compared to large all-fast systems, where the spectrum closely approaches the equilibrium spectrum throughout a major part of the assembly, coupled fast-thermal systems offer greater difficulties to a calculational treatment. Here the neutron spectrum shows a strong space dependence, especially in the low energy region, and steep flux gradients occur so that certain standard methods (e.g. diffusion approximation) may not be adequate. Therefore, an analysis of experiments on fast-thermal systems is expected to give some general insight into the applicability and limitations of various calculational methods.

Besides this, a discussion of the results may also help to answer the question, under which conditions reactor physics data of all-fast systems (e.g. spectral indices, reactivity worths of samples etc.) can be obtained from experiments on fast-thermal assemblies.

2. Description of the Reactor

The basic geometrical structure of STARK is shown in Fig.1. The fast core (37.2 cm average diameter) is formed by an array of 37 vertical stainless-steel matrix tubes which are fixed by a bottom grid plate. The tubes can be filled with platelets (5.1 by 5.1 cm) of various core materials (cf. sec. 3). In order to prevent strong peaks in the ^{235}U-fission rate at the edge of the fast zone, the core structure is enclosed in a 5 cm-thick natural uranium casing which absorbs slow neutrons incident from the driver zone. Thus, coupling between the zones is maintained mainly by the exchange of fast neutrons.

The thermal core consists of up to 370 Argonaut-type fuel plates and light water as a moderator. The fuel plates, each of them containing 20.83 g ^{235}U (20 percent enriched), are arranged in 24 groups with a 6.3 mm spacing inside an annular aluminium tank; the volume between the fuel region and the outer tank wall is filled with graphite plates and wedges. Normally the thermal zone is operated at 80°C in order to guarantee a high degree of inherent shutdown capability of the reactor.

The control system acts primarily upon the thermal driver zone. Twelve cadmium-plate control units are evenly distributed around the thermal core and provide a total shut-down reactivity of at least 2 %k. Three of them can be used as fine-control units. An additional fuel-poison safety rod is installed at an eccentric position in the fast core. It consists of a vertically driven matrix tube which is filled with the normal core materials and to the upper part of which a boron carbide absorber is attached.

The regular neutron instrumentation is conventional. It comprises several ionisation chambers and BF_3-counters located in the graphite reflector. Additional neutron detectors for experiments can be placed into various channels of the reactor and into specially loaded matrix tubes of the fast core.

A more detailed description of STARK and its safety aspects is given in an earlier paper [1].

3. Core Configurations

Up to now, four reactor configurations have been investigated which differ largely in the material composition of the fast core and the number of fuel plates in the thermal zone.

In the first assembly the matrix tubes of the central zone were filled with natural uranium metal. Since the contribution of fast fissions to the total reactor power was only about 5 percent, this configuration may still be considered as an all-thermal system.

With the following assemblies the amount of fuel in the fast zone was raised stepwise up to 107 kg ^{235}U, while the ^{235}U-content of the thermal zone had to be reduced from 7.6 kg to 4.5 kg ^{235}U to keep the system critical. With the most reactive fast core a fast fission contribution of ≈ 40 percent was reached so that the dependence of reactor parameters on the reactivity partition of the fast core could be studied over a relatively large interval.

The core materials for STARK are 3.15 mm-thick platelets of natural uranium, 20 percent enriched uranium, aluminium, and aluminium oxide, which are stacked horizontally inside the matrix tubes. As shown in Fig.2, relatively simple loading patterns have been chosen and no attempt has been made, because of the limited number of materials available, to simulate more "realistic" fast reactor core compositions.

In Assembly 2, a small amount of polyethylene (H/U-ratio = 0.053) was added to the fast core in order to obtain a soft neutron spectrum similar to that of a steam-cooled fast reactor. The polyethylene was used in form of discs (2.0 cm diameter, 1 mm thick) which were placed into recesses machined into the aluminium platelets. Assemblies 3 and 4 had no polyethylene admixture and were designed to render hard spectra and larger fast core power fractions. Tab.1 gives the material composition of these assemblies.

As shown in Fig.2, 8.4 cm-thick axial reflectors of natural uranium metal were arranged at both ends of the fast core region. The height of the core filling was about 60 cm. It was chosen in such a way so as to render approximately equal axial bucklings in both core regions and to make a comparison with one-dimensional radial calculations meaningful.

4. Experiments

The objective of the experimental work was to obtain data on the neutron spectra in the fast core, on the spatial distribution of reaction rates throughout the reactor, and on central reactivity worths of various sample materials. Furthermore, the variation of reactor parameters, e.g. neutron lifetime, reactivity coefficients etc., was to be studied as a function of the partition of reactor power between both core regions.

In this section the experimental methods and procedures, some of them standard techniques, are outlined briefly. A discussion of the results and a comparison with calculations is then given in the following section. Some of the more recent experimental methods used at STARK are described in a separate paper [4].

4.1 Approach to Critical

For each assembly a critical configuration with given geometry and material composition of the fast zone was to be established, whereas the number of fuel plates in the thermal region was taken as a free parameter to adjust criticality.

The approach to critical usually started from a configuration in which the fast zone was completely filled with natural uranium and the thermal zone with about 80 percent of the critical fuel loading predicted by multigroup calculations. Then the natural uranium elements were replaced with loaded fast core elements. The thermal core was filled with moderator and half of the control plates were withdrawn to ensure complete control of multiplication during the loading process. Finally, the loading of the thermal zone was completed until the reactor went critical.

The critical masses of the thermal zone are listed in Tab.2 for the various assemblies. Agreement with calculated values was found within $\pm$ 6.5 percent.

4.2 Measurement of Reaction Rates

4.2.1 Fission Rates

Three different methods were employed to determine fission rates in the fast zone of STARK:

(a) using parallel-plate absolute fission chambers,

(b) using small cylindrical fission chambers,

(c) by γ-counting of irradiated uranium foils.

In the thermal zone only measurements with a 3 mm-diameter ^{235}U-chamber could be made because of the small spacing between the fuel plates. However, pairs of gold and copper foils were irradiated there to investigate axial, radial, and azimuthal distributions of the thermal and epithermal neutron flux.

As a basis for a calibration of the other counters, absolute measurements with parallel-plate fission chambers were performed in the center of the fast core. The chambers (4.0 cm diameter, 0.5 cm plate spacing) were similar to those described by KIRN (5) and were operated as flow counters with an argon-methane mixture. Two of these counters were placed back-to-back in a void volume inside the central matrix tube. The layers of fissionable material were commercially available samples of ^{232}Th, ^{233}U, ^{235}U, and ^{238}U ($\approx 300\ \mu g/cm^2$ thick) of gravimetrically known mass *), which was found to agree with low-geometry α-counting within $\pm$ 1 percent for ^{233}U and within $\pm$ 3 percent for ^{238}U (Tab.3). A calibration by absolute β-γ-coincidence counting of a gold foil irradiated close to the sensitive area of the counter in the thermal column of the reactor gave 6 percent lower effective masses, probably due to fission fragment losses in the sample layer. Therefore, the absolute values of the fission rates and ratios should be considered as preliminary until measurements with thinner samples have been made.

To study the spatial distribution of fission rates in the fast zone, small cylindrical fission chambers (20th Century Electronics, FC-4, 6 mm outer diameter) were used which were coated with ^{232}Th, ^{233}U, ^{235}U, ^{238}U, ^{237}Np, and ^{239}Pu. The coating thickness was in the order of $500\ \mu g/cm^2$. These chambers were calibrated against the parallel-plate absolute fission chambers in the center of the fast core or, in case of ^{237}Np and ^{239}Pu, with a 14 Mev neutron generator of known intensity.

*) The foils were fabricated and weighed by the EURATOM Central Bureau for Nuclear Measurements, Geel, Belgium.

Four cylindrical chambers were combined to a unit which was introduced into a 1.8 cm-wide vertical channel spared out in one of the matrix tubes or in the natural uranium zone, so that they were exposed to nearly the same neutron field and data of four substances could be taken simultaneously. For the measurement of axial traverses the chambers could be moved vertically by an automatic driving mechanism. Radial traverses were also obtained by using different matrix positions.

Some results of the fission chamber measurements are given in Fig.3 to 5. The ordinate values are fission rates n^x per atom in material x ($x = {}^{235}U$, ${}^{238}U$), normalized to a reactor power of 1 watt. Fig.3 shows an axial ${}^{235}U$-traverse taken in Assembly 4 between the fuel plates of the thermal zone at a distance r = 34.8 cm from the center. An approximate cosine shape was found in the core region, except for perturbations close to the axial water reflectors and a bump at 2 cm below the reactor midplane which is caused by an annular water channel in the graphite pieces around the fuel region. A cosine function was fitted to the unperturbed parts of the curve, leading to an effective core height $H_{eff} = 85.0 \pm 2$ cm.

Axial traverses in the central position of the fast core are shown in Fig.4. Tab.4 gives the effective core heights obtained by fitting cosine functions to the traverses. Deviations of ≤ 3.5 cm from the H_{eff}-value in the thermal zone were found. Also it is noted that in both core regions the maximum of the fission distribution is shifted by ≈ 1 cm towards the bottom with respect to the geometrical reactor midplane, probably due to control-plate shadowing and neutron losses in the slightly conical air gap at the outer wall of the thermal core.

Radial ${}^{235}U$- and ${}^{238}U$-traverses measured in the reactor midplane of Assembly 4 are plotted in Fig.5. In addition to the fission chamber data, the ${}^{235}U$-fission rate in the thermal zone was also derived from the thermal flux Φ_{th} and the epithermal flux Φ_{ep} per unit lethargy at 4.9 ev found by the Au+Cu-foil activation:

$$n^{25}(r) = \sigma_{th}^{25}\, g^{25}\, \Phi_{th} + \sigma_{ep}^{25}\, \Phi_{ep}\,, \qquad (4.1)$$

where $\sigma_{th}^{25} = 582$ barn = thermal fission cross section of ${}^{235}U$,

$g^{25} = 0.962$ = Westcott factor for ${}^{235}U$ at $80^{\circ}C$;

the effective epithermal fission cross section

$$\sigma_{ep}^{25} = \frac{\sum_{i=1}^{25} \phi_i \, \sigma_i^{25}}{\phi_{21}/\Delta u} = 429 \text{ barn} \qquad (4.2)$$

was determined from the calculated 26-group fluxes ϕ_i in the thermal zone ($\phi_{21}/\Delta u$ = flux per unit lethargy at 4.9 ev, i.e. in group 21).

The radial distribution of the ^{235}U-fission rate, n^{25}, shows a steep gradient in the natural uranium and the outermost region of the fast core due to the strong absorption of slow neutrons coming from the thermal zone. In the inner region of the fast core relatively flat shapes of the ^{235}U- and ^{238}U-fission rates are found.

From the fission rates n^{25}, n^{28}, the number of fissions Z per unit volume in the actual reactor is derived,

$$Z(r) = N^{25} \, n^{25}(r) + N^{28} \, n^{28}(r) \, , \qquad (4.3)$$

where N^{25}, N^{28} = number of ^{235}U- and ^{238}U-nuclei per cm^3 of the core mixture (Tab.1).

Integration of Z(r) leads to the power contributions

$$\gamma_i = \bar{Z}_i / \sum_{\text{all zones}} \bar{Z}_i \, , \qquad \bar{Z}_i = 2\pi \int_{\text{zone i}} Z(r) \, r \, dr \qquad (4.4)$$

of the various zones, which are compared in Tab.2 with calculated values.

4.2.2 ^{238}U-Capture-to-Fission Ratio

Capture-to-fission ratios have been determined by irradiation of 0.1 mm-thick uranium foils at different positions between the platelets of the fast core and subsequent γ-counting of both the induced ^{239}Np- and fission product activities.

To separate the γ-activity caused by neutron capture in ^{238}U from the fission background, the γ-x-ray cascade of ^{239}Pu at 105 kev was observed by a coincidence technique in connection with an absolute calibration using the α-decay of ^{243}Am as a standard. This method is described in a separate paper [4] of this conference. At the same time, fission product γ-activities

above 660 kev, which are proportional to the fission rate, were measured and the contributions of ^{235}U and ^{238}U were separated by using foils of different enrichment. A calibration of the foil activities in terms of absolute fission rates was achieved by a comparison with parallel-plate fission chambers.

Foil counting and data processing were carried out with an automatic sample changer [6] in connection with a computer code, both specially developed for work with a large number of fission foils.

Fig.6 shows some of the experimental results found for Assembly 4 in comparison with the 26-group calculations (cf. 5.2).

4.2.3 Measurements with Resonance and Threshold Detectors

Additional information on the neutron spectrum in the ev- and kev-region was obtained from an investigation of (n,γ)- and (n,n')-reaction rates found by the foil activation technique.

In Assembly 2 and 4 several indium foil measurements were performed, employing the reactions $^{115}In(n,\gamma)^{116m}In$ (first resonance at 1.46 ev), $^{113}In(n,\gamma)^{114m}In$ (main resonances at 4.7, 14.7, 21.7, 25.2, and 32.5 ev), and the reaction $^{115}In(n,n')^{115m}In$ (threshold at 335 kev). The foils were irradiated inside 0.6 cm-thick aluminium drawers which were embedded in the normal plate structure of the fast core at different matrix positions. The decay of the foil activity was observed with 2π-ß-counters and analyzed, on the basis of the known half-lives, for the contributions of the three reactions to saturation activity.

The radial traverses of the reaction rates in Assembly 4 (Fig.7) show a fairly good agreement with the 26-group diffusion calculation in case of the (n,n')-reaction, but larger discrepancies for the resonance reaction $^{115}In(n,\gamma)$ which are discussed in sec. 5.2.

Experiments were also made with indium sandwiches, composed of three identical foils, in order to determine the contribution of the 1.46 ev-resonance to the total foil activity. The experimental activity-ratio of outer to inner foil, C_o/C_i, is compared in Tab.5 with values calculated from the 26-group spectra (cf. 5.1) on the basis of the known $^{115}In(n,\gamma)$-cross section, neglecting the effect of Doppler-broadening. The experimental

quantity $C_o/C_i - 1$, which increases with the ratio of the resonance flux at 1.46 ev to the total $^{115}In(n,\gamma)$-reaction rate, is found to be 3 to 6 times as high as calculated, showing that the intensity of ev-neutrons in the spectrum is much higher than expected from theory.

Further measurements to check the spectrum in the kev-region were made in Assembly 2, using the resonance detectors ^{19}F, ^{23}Na, and ^{27}Al. The foil materials, their dimensions, the experimental set-up including the rabbit irradiation system, and the procedure of data evaluation are described in (4). Irradiations of NaF-foils were performed inside the loaded matrix tubes (positions 19, 25, 30, Fig.1) of the fast core and in the empty channel of the natural uranium zone. The foils were covered by 1 mm Cd to prevent activation by thermal neutrons. The irradiation of "Teflon" (^{19}F)- and Al-foils was performed in the empty matrix positions 19 and 34 by means of the pneumatic rabbit system.

The activation integral from Cd-cutoff to the maximum fission energy has been chosen as a basis for comparison of experimental and theoretical results. Fig.8 shows the activation integral derived from foil activities and the 26-group diffusion calculation as a function of radial position in the reactor midplane. The calculations have shown that in the spectrum of Assembly 2 the activation due to neutrons in the energy region of the main resonance compared to the activation due to all other neutrons is $\approx$ 81% for ^{23}Na (main resonance at 2.95 kev), 63% for ^{19}F (main resonances at 15.3 and 27.3 kev), and for ^{27}Al $\approx$ 46% (first resonance at 5.9 kev) and $\approx$ 16% (second resonance at 35.0 kev). The calculated curves were normalized at r = 0 to the experimental points. The experimental value at r = 19.3 cm in Fig.8 is too large because the irradiation was made in the empty channel. The approximate shape of the curve in the full channel is also indicated (dashed-dotted line).

Experimental and calculated curves agree in their shapes fairly well in case of ^{23}Na and ^{19}F, indicating no larger discrepancies between calculation and experiment in the kev-region of the spectrum. The relatively large deviation for ^{27}Al is believed to be of systematic nature and has to be investigated further.

4.3 Differential Spectrum Measurements with Spherical Hydrogen Counters

Differential neutron spectra were measured in the fast core of Assembly 4 by the proton recoil technique using hydrogen-filled spherical proportional counters*) [7]. Four counters, each 4 cm in diameter, with different fillings and pressures were used to cover the energy range from 25 kev to 1 Mev (Fig.9). The γ-n-discrimination technique [8], by which the low energy limit of the 1 atm-hydrogen counter could be lowered, was not employed in the measurements performed so far.

Spectra were measured in the reactor midplane at various radial positions where the counter was placed in an empty volume inside the matrix tube. By operating the reactor at a low power level (≈ 10 mW), the counting rate was kept below 2000 cps so that deadtime losses could easily be corrected for by the live timer of the analyzer.

The well-known relationship

$$\emptyset(u) = E\,\emptyset(E) = -\frac{E^2}{N\,T\,\sigma(E)}\,\frac{dD(E)}{dE} \qquad (4.5)$$

was used to convert the measured distribution of recoil protons per unit energy, D(E), into the neutron flux Ø(u) per unit lethargy. σ(E) is the known n,p-scattering cross section, N the number of hydrogen atoms in the sensitive region of the detector, and T the live counting time. The energy calibration was made with monoenergetic neutrons from a Van-de-Graaff using the $^{7}Li(p,n)^{7}Be$-reaction.

To analyze the counting data on the basis of eq.(4.5) a computer code was used, which determines the logarithmic derivative of D(E) and its error from a section of the experimental proton recoil distribution. The slope-taking interval was chosen to be 25 percent, i.e. about twice the energy resolution of the detectors.

Wall-effects were corrected for, as described by BENJAMIN [7], by first subtracting from the measured recoil spectrum the contribution of neutrons with energies above the upper limit of the counter, as calculated by a Monte-Carlo code, and then multiplying the slope of the resulting recoil distribution with wall-effect factors, also derived from Monte-Carlo calculations.

In Fig.9 the experimental and calculated spectra are compared for the central position of Assembly 4.

*) Counters fabricated by 20th Century Electronics, Great Britain.

4.4 Reactivity Measurements

4.4.1 Methods

To determine larger reactivity worths ($|\Delta\varrho| \gtrsim 0.05$ ß) in STARK, positive period, rod-drop, and "continuous run" [9] techniques have been employed. For measurements of central reactivity worths of small samples also a square-wave pile-oscillator was used. In all cases the time-dependence of the neutron population n(t) was observed and subsequently analyzed on the basis of the space-independent reactor model.

The neutrons were detected by a ^{10}B- or ^{3}He-ionization chamber normally located near the thermal core in the graphite reflector. The chamber signal was amplified by an electrometer amplifier (Keithley, Model 417) and then fed to a voltage-to-frequency converter, the output of which consisted of a pulse chain with frequency proportional to the input signal. The pulses were counted in a 256-channel multiscaler time analyzer (TMC, Model CN-110).

4.4.2 Calibration of Control Plates

For a fast and reliable control plate calibration the rod-drop technique was found to be advantageous. Basically, the reactivity change was determined by comparing the experimental decay of the neutron signal n(t) with a set of n(t)-curves calculated for various reactivities.

For a source-free point-reactor, the neutron signal after a step change in reactivity applied at t = 0 to the stationary and critical reactor is given by

$$\frac{n(t)}{n_o} = \sum_{j=0}^{N} A_j \, e^{s_j t} \quad , \tag{4.6}$$

where n_o is the initial neutron signal at critical,

s_j are the solutions of the inhour equation

$$s \left(\Lambda + \sum_{i=1}^{N} \frac{ß_{eff\ i}}{s + \lambda_i} \right) - \varrho = 0 \quad , \tag{4.7}$$

Λ is the prompt-neutron generation time,

$ß_{eff\ i}$, λ_i are the delayed neutron parameters,

$$A_j = \frac{\Lambda + \sum_{i=1}^{N} \frac{\beta_{eff\,i}}{s_j + \lambda_i}}{\Lambda + \sum_{i=1}^{N} \frac{\beta_{eff\,i}}{(s_j+\lambda_i)^2}} \quad , \tag{4.8}$$

and N is the number of delayed neutron groups. Because of the difference in the λ_i-values for ^{235}U and ^{238}U (10), 12 delayed neutron groups were used, six for each isotope. The effective parameters $\beta_{eff\,i}$ were derived from a 26-group perturbation calculation (cf. sec. 5.1 and Tab.2).

A detailed analysis of the experimental n(t)-curves revealed a strong variation in the amplitude of the prompt transient with detector position, whereas a few seconds after completion of the reactivity change a common, space-independent time-behavior was found. To eliminate spatial effects from the experimental data, n(t) was normalized not to the initial value n_o but rather to a value n(T) some seconds after the drop ($T \gtrsim 5$ sec) which is not influenced by higher modes. The reactivities ρ/β_{eff} were obtained by comparison of the experimental ratios n(t)/ n(T), (t > T), with those calculated by eq.(4.6) and were found to be independent of detector position within $\pm$ 2 percent.

Compared to the space-independent model, the prompt transient is larger for detector positions close to the control plate and smaller for positions far away. On the boundary of both regions, positions exist (at an azimuthal angle of $\approx 60^o$ from the plate) where n(t) was found to agree well with the space-independent calculation in its entire time-dependence. In these positions complete control plate characteristics were determined by the continuous-run technique in a single experiment and no systematic deviations from the other methods were seen.

Tab.2 and Fig.10 show some results of the reactivity measurements for the safety-rod S_4 in the fast zone and for various groups of control plates (Fig.1). A decrease of the thermal control plate worths and an increase for the rod S_4 are noted as the power contribution of the fast core grows. The worth per control plate is seen to increase initially with the number of plates inserted and then to decrease again for larger numbers. This negative coupling effect, which results from a flux-shifting towards the fast zone, increases with the importance of the fast zone.

4.4.3 Reactivity Coefficients in the Thermal Zone

For investigating the inherent shut-down mechanisms of the thermal zone, the overall reactivity effects of moderator temperature and void formation were measured.

The temperature coefficient was determined by continuously increasing the moderator temperature while the reactor was kept critical with a calibrated control plate. The calibration was performed in the same experiment by stepwise withdrawal of the plate and determination of the positive period.

In order to measure the reactivity effect of voids in the light-water moderator, a flat aluminium tube (cross section 0.4 x 1.0 cm^2) was placed between two fuel plates, and the reactor was made critical while the tube (volume $\Delta V = 24\ cm^3$) was filled with air. By a sudden pressure release water was allowed to enter the tube and the resulting reactivity $-\Delta\varrho$ was derived from a period measurement. The moderator void coefficient $\frac{\Delta\varrho}{\Delta V}$ was found to be negative throughout the thermal core.

Results of the average void coefficient $\frac{\Delta\varrho}{\Delta V}$ and the temperature coefficient $\frac{\Delta\varrho}{\Delta T}$ are given in Tab.2.

4.4.4 Reactivity Worth Measurements with a Pile Oscillator

Measurements of reactivity worths of small material samples (3 to 300 g) in the central channel of the fast zone have been carried out with a pile-oscillator for a number of substances. The samples were fixed inside an aluminium tube which was connected to the piston of a driving mechanism actuated by compressed air. The stroke of the oscillator was 40.5 cm so that the sample could be moved from the center of the core to a position outside the blanket. The transient time between both positions was 0.1 to 0.2 sec such that the reactivity changed in a square-wave manner with a period $T = 25.4$ or 38.4 sec.

In order to study the effect of neutron streaming through the empty channel, measurements were performed at Assembly 4, where the oscillating aluminium tube was substituted by a square stainless steel tube filled with 4.6 by 4.6 cm platelets of either core material or aluminium. Two aluminium containers, one for the sample and the other empty, were embedded in the oscillator rod at the two positions corresponding to the core center. With this apparatus the transient time was ≈ 1 sec and the period chosen as 64 sec.

The oscillation of the neutron flux was detected by a ^{10}B-ionization chamber placed near the core-reflector interface. The DC-part of the chamber signal was suppressed and only the oscillating part was recorded, as described in 4.4.1, by a 256-channel time analyzer which was synchronized with the oscillator in such a manner that two consecutive periods were stored in each analyzer sweep. In this way the presence and the influence of a drift component on the signal could be observed. The mean reactor power was 10 watts; small reactivity drifts during the experiment were compensated by a slowly-moving fine-control rod.

The experimental data were Fourier-analyzed on the IBM-7074 digital computer. From the Fourier amplitude, c, of the fundamental frequency $\omega = 2\pi/T$ the reactivity amplitude $\Delta = \rho/2$ of the sample was derived (assuming a square-wave oscillation) by the expression

$$\Delta = \frac{\pi}{4} \frac{c \Lambda}{n_o G_o(j\omega)} , \qquad (4.9)$$

where Λ = generation time,
n_o = mean power level,
$G_o(j\omega)$ = calculated reactor transfer function.

In an ideal square-wave oscillation only odd harmonics should be present. In the actual experiment, however, also even modes are excited by reactor noise and by the neutron scattering effect during the sample motion. When the oscillator tube is filled with core material, a strong additional component of twice the fundamental frequency is observed, which is caused by the periodical removal and reinsertion of irradiated fuel containing delayed-neutron precursors. All these effects, however, are easily eliminated by the Fourier analysis since they do not contribute to the fundamental mode of the oscillation.

The theoretical sensitivity of the oscillator experiment was calculated to be $1.2 \cdot 10^{-7}$ $\Delta k/k$ for an integrated power of 10^4 watt sec if only reactor noise is the limiting factor [11]. Measurements without sample oscillation gave 1 to 3 times this value.

Tab.7 gives the experimental reactivity coefficients of several materials compared with calculations based on a first-order perturbation theory. Effects of sample size on the reactivity coefficient were found for CH_2, B_4C, Ni, C, and (less pronounced) for U (19.2 % enriched) and U_{nat}. They were eliminated by extrapolation to zero sample mass.

The comparison of sample worths (relative to ^{235}U) for Assembly 4 in the empty channel (ρ_{empty}) and the channel filled with core material (ρ_{core}) shows remarkable differences (Tab.7), especially for the scattering materials Al, C, and CH_2. These differences are due to the anisotropy of the neutron flux $\phi(\vartheta)$ and the adjoint $\phi^+(\vartheta)$ in the empty channel, which leads to a negative net reactivity change even for a pure isotropic scatterer at the reactor center. The measured differences were found to be approximately proportional to the importance-weighted transport cross section

$$\rho_{empty} - \rho_{core} = \text{const} \sum_{i=1}^{26} \phi_i^+ \sigma_{tr\,i} \phi_i \qquad (4.10)$$

of the sample material, as obtained from the perturbation code (cf. 5.2), so that corrections could be made on this basis for the empty-channel measurements in Assembly 2 and 3 (Tab.7).

4.5 Kinetic Experiments

Pulsed source and noise analysis techniques were employed to study the variation of the prompt-neutron decay constant and the generation time with reactor configuration.

In the pulsed source experiments a periodical sequence of d,t-neutron bursts was injected into the system and the decay of the prompt neutron population, as observed with a BF_3-counter in the air gap between thermal core and reflector, was analyzed for the decay constant α of the fundamental mode. The experimental set-up and the data evaluation procedure were the same as described in (12) for previous measurements.

The decay constant α, which is related to reactivity ρ/β_{eff} and generation time Λ by

$$\alpha = \frac{\beta_{eff}}{\Lambda} (1 - \rho/\beta_{eff}) , \qquad (4.11)$$

was measured in Assembly 1 to 4 at delayed critical and at several subcritical states obtained by inserting various groups of control plates (Fig.1) into the critical reactor. The experimental α-values are shown in Fig.11 as a function of ρ/β_{eff}. The reactivity scale was determined by the rod-drop method (4.2), which is known to be insensitive to changes in generation time.

The curvature of the α-vs.-reactivity curves, increasing in magnitude from Assembly 1 to 4, shows that the generation time Λ decreases with subcriticality, due to the shielding of the thermal core and the reflector when cadmium plates are inserted. The inverse effect is observed when the system is made subcritical by insertion of the safety rod S_4 into the fast zone, by which the thermal core gains importance and the generation time grows.

Fig.11 also shows the values $\gamma = \beta_{eff}/\Lambda$ found by the method of GARELIS and RUSSEL [13] from the prompt- and delayed-neutron intensities, $n_p(t)$ and $n_d(t)$, as solution of the equation

$$\int_0^\infty n_p(t)\ (e^{\gamma t} - 1)\ dt = \int_0^\infty n_d(t)\ dt \quad . \qquad (4.12)$$

Except for Assembly 2 the γ-values vary only slightly, due to an appropriate choice of detector position, and converge against the decay constant $\alpha_c = \beta_{eff}/\Lambda_c$ measured directly at delayed critical.

Besides the pulsed source measurements also noise analysis experiments have been performed with the two-detector crosspower spectral density technique [12, 14], the Rossi-α method and the probability distribution technique [4, 12]. The results for the prompt-neutron decay constant (fundamental mode) at delayed critical found by the four methods are given in Tab.8. The data agree within the error limits.

5. Discussion of the Results

5.1 Multigroup Calculations

As a basis for a discussion of the experimental results a number of one-dimensional multigroup calculations have been performed for the various STARK assemblies, using the Russian 26-group ABN-cross-section set [15].

Most calculations were done in cylindrical geometry where the reactor was treated as a system of seven concentric zones, equal in area and material composition to the corresponding actual zones of the reactor:

Zone 1 : fast core

zone 2 : natural uranium zone

zone 3 : graphite, Al-tank walls, air gap

zone 4 : thermal core

zone 5 : graphite inside the annular tank

zone 6 : tank walls, air gap, graphite

zone 7 : external graphite reflector.

Tab.1 gives the geometry of the zones and the atom numbers per cm^3 of the homogeneous mixture as derived from the material weights.

A constant axial buckling $B_z^2 = 14.68 \cdot 10^{-4}\ cm^{-2}$ independent of zone and energy group was assumed, which corresponds to the effective core height $H_{eff} = 82$ cm found by fission chamber traverses in the thermal core of Assembly 2. Experimental H_{eff}-values of the other assemblies deviate up to 4 cm from this value (Tab.4).

The calculations were carried out with the Karlsruhe nuclear code system NUSYS [16]. As a first step, a diffusion calculation was performed to obtain spectra and reaction rates throughout the reactor. In order to find a critical system with given radius and material composition of the fast core, the thickness of the thermal zone was varied by radius iteration, taking into account the dependence of the average fuel concentration on the zone thickness due to the geometry of the graphite wedges (Fig.1). The results were carefully checked for influences of mesh width and number of iteration steps.

Then a perturbation calculation was made to derive the overall neutron generation time

$$\Lambda = \frac{\int \sum_{i=1}^{26} \Phi_i^+ \frac{1}{v_i} \Phi_i \, dV}{\int \sum_{i,j=1}^{26} \Phi_i^+ \chi_i \nu\Sigma_{f_j} \Phi_j \, dV} \qquad (5.1)$$

and the effective delayed neutron fractions of the fissionable isotopes ^{235}U and ^{238}U,

$$\beta_{eff\ k}^M = \beta_k^M \frac{\int \sum_{i,j=1}^{26} \Phi_i^+ \chi_{i_k} \nu\Sigma_{f_j}^M \Phi_j \, dV}{\int \sum_{i,j=1}^{26} \Phi_i^+ \chi_i \nu\Sigma_{f_j} \Phi_j \, dV}, \qquad (5.2)$$

where

$\beta_{eff\ k}^{M}$, β_{k}^{M} = effective and actual delayed-neutron fractions of material M, kinetic group k,

$\Sigma_{f_j}^{M}$ = macroscopic fission cross section of material M, energy group j,

χ_{i_k} = energy distribution of the delayed neutrons, kinetic group k.

Some of the resulting kinetic parameters are given in Tab.2.

Furthermore, the relative importance α_m of the core zones (index m) has been evaluated, using the equation

$$\alpha_m = \frac{\int_{\text{zone m}} \sum_{ij} \phi_i^+ \chi_i \nu \Sigma_{f_j} \phi_j \, dV}{\int_{\text{reactor}} \sum_{ij} \phi_i^+ \chi_i \nu \Sigma_{f_j} \phi_j \, dV} . \qquad (5.3)$$

The α_m are identical with the coefficients of reactivity partition in the theory of coupled systems [17] and describe the effect on the overall reactivity,

$$\Delta\rho = \sum_m \alpha_m \frac{\delta \nu_m}{\nu_m} , \qquad (5.4)$$

of a fictitious change $\delta \nu_m$ of the number of fission neutrons in zone m. As shown in Tab.2, the importance α_1 of the fast zone varies between 0.0122 (for Assembly 1) and 0.4924 (for Assembly 4).

Also reactivity worths of different materials were determined by the perturbation code. The sample volume (usually at core center) was assumed to be filled with the normal core mixture to which the sample material was added in low concentration (10^{20} to 10^{21} atoms/cm^3). In this way, the ideal worth of an infinitely small and dilute sample should be obtained and effects resulting from a variation of the resonance self-shielding factors should be excluded. Tab.7 shows results for the central reactivity worths of various sample materials, relative to ^{235}U.

Similar calculations were made for critical all-fast systems of cylindrical shape, having the same composition as the fast zone of STARK. These assemblies are large enough to render an equilibrium spectrum in the inner core region such that deviations of the STARK spectrum from the equilibrium spectrum can be studied. In addition, S_4-calculations with isotropic downscattering were carried out for STARK in order to get some information about the magnitude of systematic errors arising from the diffusion approximation.

5.2 Neutron Spectrum and Reaction Rates

The general behaviour of the neutron spectrum in STARK is illustrated in Fig.12, where the calculated 26-group spectra are given for various radial positions r in Assembly 2. The spectrum in the thermal zone follows roughly a 1/E-shape. With penetration into the fast zone, a strong decrease of low energy neutrons ($E \lesssim 100$ ev) is seen, especially for the thermal group and at the main ^{238}U-resonance (group 21), whereas the fast and intermediate neutrons show a relatively flat spatial distribution.

In the inner region of the fast core, the spectrum ϕ_i gradually approaches the equilibrium spectrum ϕ_i^{as}, as calculated for the critical one-zone system. The relative deviation $(\phi_i - \phi_i^{as})/\phi_i^{as}$ from the equilibrium spectrum, also given in Fig.12 as a function of energy, indicates a surplus of slow neutrons ($E < 1$ kev) and of fission neutrons with respect to ϕ_i^{as} near the edge of the fast core. With further penetration into the core, these excess neutrons die out and a gradual softening occurs in the main part of the spectrum (1 kev to 1 Mev). In the center of Assembly 2, the equilibrium spectrum is not yet completely reached, and deviations from ϕ_i^{as} of the order of 10 percent still remain for energies above 10 ev.

Fig.13 gives the same diagram for Assembly 4, which has a higher ^{235}U-content and, therefore, leads to a faster decay of the spatial transients. Larger deviations of the central spectrum $\phi_i(0)$ from the equilibrium spectrum are only seen in the low energy region; they are less than 2 percent in the main part of the spectrum ($E \gtrsim 10$ kev) where 99 percent of the ^{235}U-fission processes occur.

The results of the S_4-calculation included in Fig.12 and 13 show that the number of slow neutrons in the fast zone is up to 80 percent higher than given by diffusion theory, especially in those energy regions where the spectra differ strongly from ϕ_i^{as}, i.e. where strong spatial gradients are present. Above 10 kev, a good agreement between S_4- and diffusion calculations is found for the central region of the fast zone.

A direct comparison between calculated and experimental spectra in the energy range from 20 kev to 1 Mev has been made for Assembly 4 where hydrogen counter data are available. The experimental spectrum (Fig.9) shows resonance dips caused by the aluminium contained in the fast core, which are not

seen in the 26-group spectrum because of its rough group structure. The experimental spectrum appears to be somewhat softer than the calculated one.

Further information on the neutron spectrum and its spatial variation can be gained from an analysis of reaction rates in a set of different substances.

The radial distribution of fission rates found with the cylindrical fission chambers (cf. 4.2.1) is compared in Fig.14 with the 26-group calculation. The calculated fission rate n^x per atom of material x has been derived from the group fluxes ϕ_i and the fission cross section σ_i^x of material x according to

$$n^x(r) = \sum_{i=1}^{26} f_i^x \, \sigma_i^x \, \phi_i(r) \ , \qquad (5.5)$$

taking into account the correction factor f_i^x for resonance self-shielding in the core mixture; $f_i^x = 1$ was assumed for all materials not contained in the core. The calculated curves were normalized in such a way that the ^{238}U-fission rate coincides with the experiment in the center of the fast zone.

The experimental data are subject to two main sources of error. First, calibration uncertainties of less than $\pm$ 5 percent are estimated for the parallel-plate chambers, and of the order of $\pm$ 10 percent for the cylindrical ^{239}Pu- and ^{237}Np-chambers. The calibration errors may affect the absolute values of fission rates and ratios, but not the shape of the traverses and the variation of spectral indices from one assembly to the other. Second, the deviation of the actual zone boundaries from the cylindrical shape gives rise to an uncertainty in the effective radial distance to be attributed to the chamber position and leads to a scatter of the experimental points near the edge of the fast core.

The ^{235}U-fission rate in Fig.14 shows, as a result of the strong absorption of slow neutrons in the natural uranium and at the edge of the fast zone, a steep gradient which goes over into a relatively flat curve in the interior of the fast core. The experimental data are seen to agree with the theoretical curve for $r < 10$ cm, but in the outer region they are higher than calculated, indicating that slow neutrons penetrate deeper into the fast zone than predicted by the calculation.

As a sensitive indicator for the low-energy end of the spectrum, the $^{239}Pu/^{235}U$-fission ratio, σ^{49}/σ^{25}, is plotted in Fig.15. The maxima in the calculated curves result from the fact that thermal neutrons are more strongly absorbed in the natural uranium than ev-neutrons which cause fission at the lower Pu-resonances. Towards the center of the assembly the resonance neutrons die out and the fission ratios go over into the characteristic values of the fast spectrum. For all assemblies the experimental $^{239}Pu/^{235}U$-ratio in the natural uranium zone was found to be considerably higher than calculated, which means that the number of ev-neutrons in the spectrum is larger than expected from theory.

The same conclusion must be drawn from the $^{115}In(n,\gamma)$-reaction rate measured by foil activation (Fig.7). In order to separate the contribution of the 1.46 ev-resonance from the fast neutron effect, In-sandwiches were irradiated (cf. 4.2.3). The activity ratio C_o/C_i (outer to inner foil) shows for Assembly 2 even in the central position a measurable 1.46 ev-component which is about 9 times as high as calculated. In Assembly 4 with its higher ^{235}U-content the effect of 1.46 ev-neutrons, again higher than calculated, dies out within experimental error towards the center of the reactor.

The stronger penetration of low-energy neutrons relative to the diffusion calculation can be qualitatively explained by different effects: The deviations in the natural uranium zone may be partly due to a spectral hardening within the thermal group itself and also to the idealizations made in the effective-cross-section concept, by which the neutron transmission at energies between the ^{238}U-resonances is underestimated. The deviations in the lower ev-region at the reactor center can partly be attributed to transport effects (cf. the S_4-calculations in Fig.12 and 13); the remaining discrepancies are probably caused by a radial neutron streaming between the platelets of the fast core and, in case of Assembly 2, by the heterogeneous arrangement of the hydrogeneous material.

As a check of the neutron spectrum in the kev-region, reaction rates of $^{19}F(n,\gamma)$ (resonances at 15.3 and 27.2 kev), $^{23}Na(n,\gamma)$ (resonance at 2.95 kev), and $^{115}In(n,n')$ (threshold at 335 kev) in Assembly 2 and 4 are compared in Fig.7 and 8 with calculated radial traverses, and a fairly good agreement was found. Also the ^{238}U-capture rate, mainly originating from the kev-region because of the self-shielding of the lower resonances, is consistent with the calculation. Hence, it can be concluded that the spectrum in the kev-region does not strongly deviate from the 26-group diffusion calculation.

Information on the spectrum in the upper kev- and Mev-region is obtained from fission rates in threshold substances, such as ^{232}Th, ^{238}U, and ^{237}Np. The fission chamber traverses of these materials in Assemblies 2 to 4 (Fig.14) agree well in their shapes with the calculation. The absolute values, however, deviate from the calculation by factors of 1.15 for ^{232}Th and 1.30 for ^{237}Np. Since these factors are constant within $\pm$ 1.5 percent for the Assemblies 2 to 4, which have largely different spectra, it is not believed that these discrepancies arise from true spectrum deviations, but rather from systematic errors in the calibration of the cylindrical chambers and/or effects of finite group widths in the 26-group calculation.

In Fig.16 and 17 the radial variation of the fission ratios $^{238}U/^{235}U$ and $^{237}Np/^{238}U$ is plotted. The $^{238}U/^{235}U$-data for Assemblies 2 to 4 show, relative to the calculation, a somewhat slower transition into the characteristic values of the fast core, which is a consequence of the stronger penetration of slow neutrons. For Assemblies 3 and 4, strictly constant fission ratios are attained in the interior of the fast zone ($r < 10$ cm), which means that an equilibrium spectrum is reached in the energy region that contributes predominantly to the fission rates. The $^{238}U/^{235}U$-ratio in Assembly 2 seems to decrease slightly towards the center, as expected from the softening of the calculated spectra (Fig.12). For Assembly 1, the fission ratios vary throughout the central uranium zone and no asymptotic spectrum is reached due to the low multiplication.

The fission ratio σ^{37}/σ^{28} between the threshold substances ^{237}Np and ^{238}U in Fig.17 shows for Assemblies 2 and 3, in accordance with the calculation, almost no radial variation. For Assembly 4, a slight decrease of the $^{237}Np/^{238}U$-ratio is seen which results from a deficiency of fast neutrons ($E > 1$ Mev) relative to ϕ_i^{as} at the edge of the fast core (Fig.13). The inverse effect (much more pronounced) is noted for the data of Assembly 1.

The fission ratios in the central position of all assemblies are summarized in Tab.9. Except for the nearly constant deviations in the case of ^{232}Th and ^{237}Np, a fairly good agreement with the 26-group calculation was found for Assemblies 3 and 4. In Assembly 2 the ratios $^{239}Pu/^{235}U$ and $^{233}U/^{235}U$ are 5 percent higher than expected, due to the influence of ev- neutrons. In Assembly 1 characteristic deviations are also seen for the other fission ratios which indicate, relative to the diffusion calculation, a stronger penetration of fission neutrons from the thermal zone into the reactor center. S_4-calculations give here a better agreement with the experimental data.

The results of the reaction rate measurements can be summarized as follows: In assemblies of high fast-core multiplication the spectrum above 100 ev does not seem to deviate substantially from the 26-group diffusion calculation and a space-independent spectrum close to the equilibrium spectrum ϕ^{as} is reached in the inner region ($r < 10$ cm) of the fast core. In the lower ev-region strong flux gradients occur and the diffusion calculation underestimates the penetration of such neutrons into the fast zone. S_4-calculations do not fully account for this effect, and it is thought that the heterogeneous structure of the fast core may be a reason for that.

For Assembly 2 with moderate fast-core multiplication the spatial variation of the experimental fission ratios as well as the calculations show that ϕ^{as} is not completely reached in the center of the reactor. Resonance neutrons penetrating into the center contribute slightly to the ^{233}U- and ^{239}Pu-fission rates.

In Assembly 1 with the natural-uranium-filled central region the spectrum varies throughout the core and no equilibrium spectrum is attained at all.

5.3 Central Reactivity Worths of Samples

The investigation of reactivity worths of a set of sample materials may give further information on the neutron spectrum ϕ_i, the shape of the adjoint flux ϕ_i^+, or the nuclear cross sections of the sample materials.

The reactivity worths found with the pile oscillator in the central position of STARK are given in Tab.6, already corrected for sample size effect and scattering contribution (cf. 4.4.4). For a comparison with the 26-group perturbation calculation in Tab.7 the data for material x are normalized to the reactivity effect of ^{235}U,

$$\Delta\rho^x / \Delta\rho^{25} ,$$

in order to eliminate the influence of differences in critical mass between the actual and the calculated reactor.

Comparing experimental and calculated sample worths, much higher discrepancies are found than for the fission ratios, and only qualitative conclusions can be drawn. The only values to agree with the calculation

within ± 10 percent are the ratios Ni/^{235}U and ^{238}U/^{235}U (for Assemblies 3 and 4). For these materials the main contribution to $\Delta\rho$ comes from nearly the same energy range (group 5 to 15) of the spectrum.

The reactivity ratio of ^{10}B/^{235}U is about 30 percent higher than calculated (the ^{10}B-data of Assembly 2 are possibly affected by a sample size effect). This deviation can be explained by the higher flux of ev-neutrons (as seen from the ^{115}In-activation) which contribute to the ^{10}B-absorption rate.

The large deviations for the scattering materials Al, C, and H cannot be understood alone by spectrum or sample cross section effects. These materials are sensitive indicators for the derivative of the adjoint ϕ_i^+ with respect to energy, i.e. for the height of the ^{238}U-threshold and the position of the minimum. To explain the experimental data, a somewhat deeper minimum of ϕ_i^+, which could possibly arise from transport or heterogeneity effects, must be assumed.

5.4 Dependence of Integral Reactor Parameters on the Reactor Loading

The experimental values of various integral reactor parameters of STARK are summarized in Tab.2 together with results of the 26-group diffusion calculation.

The calculated critical fuel mass of the thermal zone is up to + 6.5 percent higher than the experimental value, which corresponds to a maximum deviation in k_{eff} of - 1.5 %k; this deviation reduces to - 1.0 %k when the S_4-approximation is used. Regarding the simplifications in the calculational treatment (e.g. homogenization of thermal core and air gaps) and the deviations of the actual zone bucklings B_z^2 from the value assumed in the calculation, the agreement in k_{eff} must be considered as satisfactory.

For Assemblies 2 and 3 also the power contributions of the core zones agree well with the calculation; the effect of an underestimation by theory of the ^{235}U-fission rate in the fast core and the natural uranium zone is nearly compensated by the lower fuel mass in the thermal zone. In Assembly 4 the power contribution of the fast zone is about 10 percent lower than calculated, which could be a consequence of the larger differences in the axial zone bucklings (Tab.4).

For the void coefficient in the thermal zone and the reactivity worth of core material in the reactor center a comparison has been made with estimated values based on a 26-group first-order perturbation calculation. These values differ by as much as $\pm$ 40 percent from the experimental ones and show also a different variation with reactor loading.

As expected from the simple two-zone model of a coupled fast-thermal reactor, the neutron generation time and the reactivity worths in the thermal core (e.g. moderator void coefficient, worth of Cd-plates) are seen to decrease considerably with increasing power contribution γ_1 (or importance α_1) of the fast zone, i.e. when going from Assembly 1 to 4. At the same time also the critical ^{235}U-content M of the thermal zone decreases. The relation between the fuel mass M and the power fraction γ_1 is given in Fig.18, and an excellent agreement between experiment and calculation is noted. Further calculations have shown that this relation between γ_1 and M is in good approximation independent of the particular fast core composition so that interpolations between the 4 assemblies can be made.

Also for a discussion of the other reactor parameters in Fig.18 the fuel mass M has been chosen as abscissa. The worth of a single cadmium control plate, Δk_{Cd}, shows a variation with M which agrees in its shape with the perturbation calculation for a thermal absorber. A stronger variation is found for the combined effect of all 12 control plates due to their mutual shadowing. The experimental data for the neutron generation time Λ were found to be 10 percent higher than the values calculated from eq.(5.1). This deviation is far beyond the experimental error and must be investigated further.

6. Conclusions

The analysis of the experimental data has shown that most of the fundamental properties of the coupled system STARK are described fairly well by diffusion calculations using the 26-group ABN-cross-section set. Satisfactory agreement was found, in particular, for the critical mass and the partition of reactor power between the various zones. Large discrepancies, on the other hand, were found for the reactivity worths of sample materials in the fast zone.

To investigate the neutron spectrum in the fast core, fission rates and differential neutron spectra were measured. For systems with sufficiently high fast-core multiplication, the fission rates are consistent with diffusion

calculations in the central region of the fast zone, whereas larger deviations were found for ^{235}U and ^{239}Pu in the natural uranium zone. These deviations indicate a stronger penetration of ev-neutrons into the fast core than predicted by diffusion theory; S_4-calculations give a better, but not yet satisfactory agreement.

Calculations and fission ratio measurements show that for sufficiently high fast-core multiplication the neutron spectrum approaches in the central region of the fast zone closely the equilibrium spectrum of an all-fast system of the same core composition. Deviations occur only at the low-energy end of the spectrum, which normally gives negligible contributions to the reaction rates.

The large discrepancies for the central reactivity worths of samples cannot be explained by spectral effects alone. Assuming that the 26-group cross sections of the sample materials are not substantially in error, it must be concluded that the energy dependence of the adjoint flux ϕ_i^+ at the center of STARK deviates from the diffusion calculation; a more pronounced minimum of ϕ_i^+ must be assumed to explain the experimental data. Further theoretical and experimental work (e.g. measurement of the neutron importance) appears to be necessary for a better understanding of these discrepancies.

The dependence of the integral reactor parameters (critical mass, neutron lifetime, power fractions of the zones) on the reactor loading were found to be in reasonably good agreement with the calculations so that reliable predictions can be made for other assemblies.

As shown by the results of this paper, useful information on neutron spectra and reaction rates in specific fast reactor systems can be obtained from experiments on coupled fast-thermal assemblies similar to STARK. However, greater effort on the theoretical and experimental side seems necessary for a quantitative evaluation of measured reactivity effects.

Acknowledgments

The authors wish to acknowledge the assistance given by the STARK operation staff during the experimental work. They also wish to thank Miss R. Kurmis for the numerical evaluation of experimental and calculated data. We also gratefully acknowledge the preparation of the fission foils by the EURATOM Central Bureau for Nuclear Measurements in Geel, Belgium.

References

(1) H.MEISTER, K.H. BECKURTS, W.HÄFELE, W.H. KÖHLER, and K.OTT, "The Karlsruhe Fast-Thermal Argonaut Reactor Concept", KFK-217, Kernforschungszentrum Karlsruhe (1964)

(2) R. AVERY et al., "Coupled Fast-Thermal Power Breeder Critical Experiment", Proc. Second U.N. International Conference on the Peaceful Uses of Atomic Energy 12, p.151-165 (1958)

(3) P.ENGELMANN et al., "Construction and Experimental Equipment of the Karlsruhe Fast Critical Facility, SNEAK", Paper presented at this Conference

(4) A.BAYER, H.SEUFERT, and D.STEGEMANN, "Special Experimental Techniques Developed Recently for Application in Fast Zero Power Assemblies", Paper presented at this Conference

(5) F.S. KIRN, "Neutron Detection with an Absolute Fission Chamber", Proc. Symp. on Neutron Detection, Dosimetry, and Standardization, sponsored by IAEA, Harwell, Vol.II, p.497 (1963)

(6) K.H. BLANK and H.SEUFERT, "An Automatic Sample Changer with a Special Changing Method for γ- and γ-γ-Active Sources", Nucl. Instr. and Meth., in press

(7) P.W. BENJAMIN et al., "The Use of a Gas-Filled Spherical Proportional Counter for Neutron Spectrum Measurements in a Zero Energy Fast Reactor", AWRE Report No. NR 2/64 (1964)

(8) E.F. BENNETT, "Neutron Spectrum Measurements in a Fast Critical Assembly", ANL, RPD-EPM Memo No. 50 (1965)

(9) S.G. CARPENTER, "Reactivity Measurements in the Advanced Epithermal Thorium (AETR) Cores", AI-8549 (1963), and also in Nucl. Sc. Eng. 21, 429-440 (1965)

(10) G.R. KEEPIN, "Physics of Nuclear Kinetics", Addison-Wesley Publishing Comp., Inc., Reading, Ma. (1965)

(11) O.R. FRISCH and D.J. LITTLER, "Pile Modulation and Statistical Fluctuations in Piles", Phil. Mag. Ser. 7, 45 (1954)

(12) M.EDELMANN, G.KUSSMAUL, H.MEISTER, D.STEGEMANN, and W.VÄTH, "Pulsed Source and Noise Measurements on the STARK Reactor at Karlsruhe", KFK-303, and IAEA-Proceedings on Pulsed Neutron Research, Vol.II, 799-824 (1965)

(13) E.GARELIS and J.L. RUSSELL, Jr., "Theory of Pulsed Neutron Source Measurements, Nucl. Sc. Eng. 16, 263-270 (1963)

(14) W.SEIFRITZ, D.STEGEMANN, and W.VÄTH, "Two Detector Crosscorrelation Experiments in the Fast-Thermal Argonaut Reactor STARK, Proc. of the Int. Symp. on Neutron Noise, Waves, and Pulse Propagation, Gainesville, Florida, February 1966

(15) L.P. ABAGJAN, N.O. BAZAZJANC, I.I. BONDARENKO, and M.N. NIKOLAEV, "Gruppenkonstanten schneller und intermediärer Neutronen für die Berechnung von Kernreaktoren", KFK-tr-144, Translation of Kernforschungszentrum Karlsruhe (1964)

(16) H. BACHMANN et al., "The Karlsruhe Nuclear Code System NUSYS", to be published

(17) R.AVERY, "Theory of Coupled Reactors", Proc. Second U.N. International Conference on the Peaceful Uses of Atomic Energy 12, p.182-186 (1958)

List of Tables

List of Figures

TAB.1 Material composition of the STARK assemblies (atom numbers per cm^3)

Zone No.	1				2	3	4	5	6	7
Zone	Fast core				Natural uranium	Graphite + air gap	Thermal Core	Graphite	Graphite + air grap	Graphite reflector
Outer radius	18.6 cm				24.2 cm	30.5 cm	38.5 to 45 cm	46.5 cm	50.5 cm	86.5 cm
Assembly	1	2	3	4	1 to 4	1 to 4	4	1 to 4	1 to 4	1 to 4
Material:										
H - 1		$1.3081 \cdot 10^{21}$				$3.680 \cdot 10^{20}$	$3.726 \cdot 10^{22}$		$2.527 \cdot 10^{20}$	
C - 12		$6.706 \cdot 10^{20}$				$4.922 \cdot 10^{22}$	$1.468 \cdot 10^{22}$	$8.526 \cdot 10^{22}$	$4.127 \cdot 10^{22}$	$8.526 \cdot 10^{22}$
O - 16		$1.1637 \cdot 10^{22}$	$1.1543 \cdot 10^{22}$	$1.4428 \cdot 10^{22}$			$2.003 \cdot 10^{22}$			
Al - 27		$1.7000 \cdot 10^{22}$	$7.695 \cdot 10^{21}$	$9.619 \cdot 10^{21}$		$9.264 \cdot 10^{21}$	$1.343 \cdot 10^{22}$		$3.484 \cdot 10^{21}$	
Fe - 56	$6.042 \cdot 10^{21}$	$6.042 \cdot 10^{21}$	$6.042 \cdot 10^{21}$	$6.042 \cdot 10^{21}$						
U - 235	$3.0318 \cdot 10^{20}$	$1.7659 \cdot 10^{21}$	$3.3863 \cdot 10^{21}$	$4.1597 \cdot 10^{21}$	$3.437 \cdot 10^{20}$		$1.0495 \cdot 10^{20}$			
U - 238	$4.1805 \cdot 10^{22}$	$2.2822 \cdot 10^{22}$	$2.9134 \cdot 10^{22}$	$2.6330 \cdot 10^{22}$	$4.739 \cdot 10^{22}$		$4.193 \cdot 10^{20}$			

TAB.2 Experimental reactor parameters of STARK compared with the 26-group diffusion calculation

		Assembly 1		Assembly 2		Assembly 3		Assembly 4		
	relative exp. error	exp.	calc.	exp.	calc.	exp.	calc.	exp.	calc.	
Criticality data:										
Fuel mass, fast core		7.84		44.59		87.23		106.90		kg ^{235}U
Fuel enrichment, fast core		0.72	0.72	7.06	7.06	10.36	10.36	13.57	13.57	atom %
Fuel mass, thermal core (20°C)	± 1%	7.30	7.759	6.53	6.911	5.56	5.829	4.43	4.429	kg ^{235}U
Deviation of calc. k_{eff} from exp.			-1.53		-1.28		-0.86		-0.01	%k
Power contributions:										
Fast core, γ_1	± 3%	2.0	1.82	9.3	8.51	20.0	19.42	31.1	33.49	%
Uranium zone, γ_2	±10%	9.2	8.14	9.6	9.15	10.2	10.07	10.9	11.36	%
Reactivity contributions:										
Fast core, α_1			1.22		7.60		24.95		49.24	%
Uranium zone, α_2			7.37		9.39		11.14		11.75	%
Reactivity worth (central element):										
Core material vs. void	± 5%			+0.028	+0.019	+0.213	+0.203	+0.483	+0.627	%k
Worth of safety rod S_4	± 3%	-0.06		-0.296	-0.30	-0.60	-0.63	-1.24	-1.17	%k
Reactivity worths, thermal core:										
Worth of outer fuel plate	± 5%	+0.075	+0.0677	+0.071	+0.0701	+0.067	+0.0653	+0.051	+0.0545	%k
Void coefficient	± 8%	-0.19	-0.235	-0.16	-0.212	-0.114	-0.165	-0.076	-0.103	%k / % void
Worth of temp.change, 80 ⟶ 20°C	± 3%	+1.05		+0.89		+0.625		+0.394		%k
Worth of 1 control plate	± 3%	-0.48		-0.44		-0.340		-0.242		%k
Worth of all 12 control plates	± 8%			-4.7		-3.5		-2.1		%k
Kinetic parameters:										
Generation time Λ	± 2%	1.20	1.123	1.13	1.078	0.94	0.902	0.75	0.655	x 10^{-4} sec
Delayed neutron fractions:										
β_{eff}^{25}			7.070		6.734		5.999		5.228	x 10^{-3}
β_{eff}^{28}			0.491		0.762		1.381		2.054	x 10^{-3}
$\beta_{eff} = \beta_{eff}^{25} + \beta_{eff}^{28}$			7.561		7.496		7.380		7.282	x 10^{-3}

TAB.3 Calibration of absolute fission chambers

Sample	Material	Gravimetric value	Low-geometry α-counting
		No. of nuclei	No. of nuclei
1	^{232}Th	$3.415 \cdot 10^{18}$	-
2	^{233}U	$7.43 \cdot 10^{17}$	$7.37 \cdot 10^{17}$
3	^{233}U	$3.16 \cdot 10^{18}$	$3.18 \cdot 10^{18}$
4	^{235}U	$8.38 \cdot 10^{17}$	-
5	^{238}U	$9.64 \cdot 10^{17}$	-
6	^{238}U	$3.74 \cdot 10^{18}$	$3.62 \cdot 10^{18}$

TAB.4 Effective core heights H_{eff} derived from ^{235}U-fission rate traverses

Assembly No.	Thermal zone	Fast zone
	H_{eff} (cm)	H_{eff} (cm)
1	83 $\pm$ 2.5	85 $\pm$ 3
2	82.5 $\pm$ 2.5	86 $\pm$ 2
3	85 $\pm$ 2	85 $\pm$ 2
4	85 $\pm$ 2	83 $\pm$ 2

TAB.5 Activity ratio C_o/C_i (outer to inner foil) for In-sandwiches compared with 26-group diffusion calculation

Material	Foil thickness	Assembly No.	Radial position r	Activity ratio C_o/C_i		exp. flux at 1.46 ev / calc. flux at 1.46 ev
				experimental	calculated	
	mg / cm^2		cm			
^{115}In	3 x 36.4	2	0	1.168±0.020	1.027	9.4
	3 x 11.3	4	0	1.038±0.020	1.001	-
	3 x 87.7	4	0	1.012±0.020	1.000	-
	3 x 89.0	4	16.2	1.396±0.020	1.147	6.9

TAB.6 Reactivity coefficients $\Delta\rho/\Delta N$ (in Δk per 10^{30} atoms) of sample materials measured in the central position of the fast zone of STARK; data corrected for sample size effect

	Assembly 2	Assembly 3	Assembly 4		
Material	Channel empty	Channel empty	Channel empty	Channel filled with Al	Channel filled with core material
Al	- 4.95 ± 0.15	- 11.9 ± 0.15	- 18.6 ± 0.2	- 13.46 ± 0.2	- 13.44 ± 0.2
^{10}B	- 281 ± 2	- 386 ± 2	- 715 ± 3	- 741 ± 3	- 821 ± 3
C	- 4.73 ± 0.15	- 12.1 ± 0.15	- 14.7 ± 0.15	- 9.83 ± 0.15	- 9.55 ± 0.15
Fe	- 5.62 ± 0.2	-	- 22.8 ± 0.3	- 17.4 ± 0.3	- 19.5 ± 0.3
Ni	- 8.0 ± 0.15	-	- 32.1 ± 0.3	- 26.6 ± 0.3	- 28.8 ± 0.3
^{235}U	+ 327 ± 2	+ 639 ± 3	+ 1115 ± 5	+ 1169 ± 5	+ 1298 ± 5
^{238}U	- 29.2 ± 0.2	- 48.8 ± 0.3	- 80.8 ± 0.5	- 74.8 ± 0.5	- 77.4 ± 0.5
B_4C	- 244 ± 2	-	-	-	-
CH_2	+ 66 ± 1	+ 46.3 ± 0.5	+ 169 ± 2	+ 202 ± 2	+ 221 ± 2

TAB.7 Central reactivity coefficients $\Delta\rho/\Delta N$ of sample materials in STARK relative to ^{235}U in comparison with 26-group diffusion calculations

	Assembly 2			Assembly 3			Assembly 4		
	experimental			experimental			experimental		
	empty channel	scattering corrected	calculated	empty channel	scattering corrected	calculated	empty channel	channel filled with core material	calculated
Al	- 0.0152	- 0.011	-0.00821	- 0.0186	- 0.013	- 0.00917	- 0.0167	- 0.0104	- 0.00724
^{10}B	- 0.860	- 0.85	- 0.765	- 0.604	- 0.60	- 0.454	- 0.641	- 0.633	- 0.489
C	- 0.0145	- 0.010	- 0.00694	- 0.0189	- 0.014	- 0.00645	- 0.0132	- 0.0073	- 0.00186
Fe	- 0.0172	- 0.0128	- 0.01192	-	-	- 0.01290	- 0.0204	- 0.0150	- 0.01224
Ni	- 0.0245	- 0.018	- 0.01864	-	-	- 0.02036	- 0.0288	- 0.0222	- 0.02084
^{238}U	- 0.0894	- 0.079	- 0.0664	- 0.0763	- 0.065	- 0.0594	- 0.0725	- 0.0596	- 0.0542
B_4C	- 0.747	- 0.74	- 0.6053	-	-	- 0.3703	- 0.605	-	- 0.3790
CH_2	+ 0.202	+ 0.213	+ 0.04455	+ 0.0728	+ 0.090	- 0.00873	+ 0.152	+ 0.170	+ 0.0857

TAB.8 Prompt neutron decay constant at delayed critical, $\alpha_c = \frac{\beta_{eff}}{\Lambda_c}$ (sec^{-1})

Assembly No.	Pulsed source method	Noise analysis methods		
		Cross power spectral density	Rossi-α	Probability distribution
	sec^{-1}	sec^{-1}	sec^{-1}	sec^{-1}
1	62.9 ± 0.8	63.4 ± 2	-	63 ± 2
2	66.4 ± 1.5	67 ± 2	71 ± 5	67 ± 2
3	78.3 ± 2	74.5 ± 2	-	-
4	96.7 ± 2	93 ± 4	93 ± 4	-

TAB.9 Fission ratios and fission-to-capture ratios in the central position of STARK compared with 26-group calculations

			Assembly 1			Assembly 2		Assembly 3		Assembly 4	
Materials	method	relative statistical error	exp.	calc. D	calc. S_4	exp.	calc. D	exp.	calc. D	exp.	calc. D
σ_f^x/σ_f^{25} :											
$^{232}Th/^{235}U$	K	± 3%	0.00196	0.00130	0.00142	0.00504	0.00436	0.00785	0.00674	0.00922	0.00793
$^{238}U/^{235}U$	K	± 1%	0.00823	0.00688	0.00747	0.0228	0.02226	0.0351	0.03427	0.0408	0.04023
$^{237}Np/^{235}U$	C	± 1%	0.145	0.1267	0.1253	0.218	0.1654	0.336	0.2541	0.375	0.2774
$^{233}U/^{235}U$	K	± 1%	-	1.600	-	1.57	1.432	-	1.490	1.52	1.492
$^{239}Pu/^{235}U$	C	± 1%	1.064	1.076	1.081	1.014	0.9847	1.054	1.110	1.071	1.123
σ_f^x/σ_f^{28} :											
$^{232}Th/^{238}U$	K	± 3%	0.238	0.1889	0.1904	0.221	0.1958	0.224	0.1968	0.226	0.1971
$^{237}Np/^{238}U$	C	± 1%	17.6	18.4	16.78	9.57	7.43	9.57	7.43	9.18	6.89
σ_c^x/σ_f^{25} :											
$^{238}U/^{235}U$	F	± 2%	-	0.1234	-	-	0.1249	-	0.1225	0.127	0.1208

K : Calibration with Kirn-type absolute fission chamber
C : Cylindrical fission chamber
F : Foil activation
D : Diffusion calculation
S_4: S_4-calculation (agrees with D within ± 0.5 % for Assemblies 2 to 4)

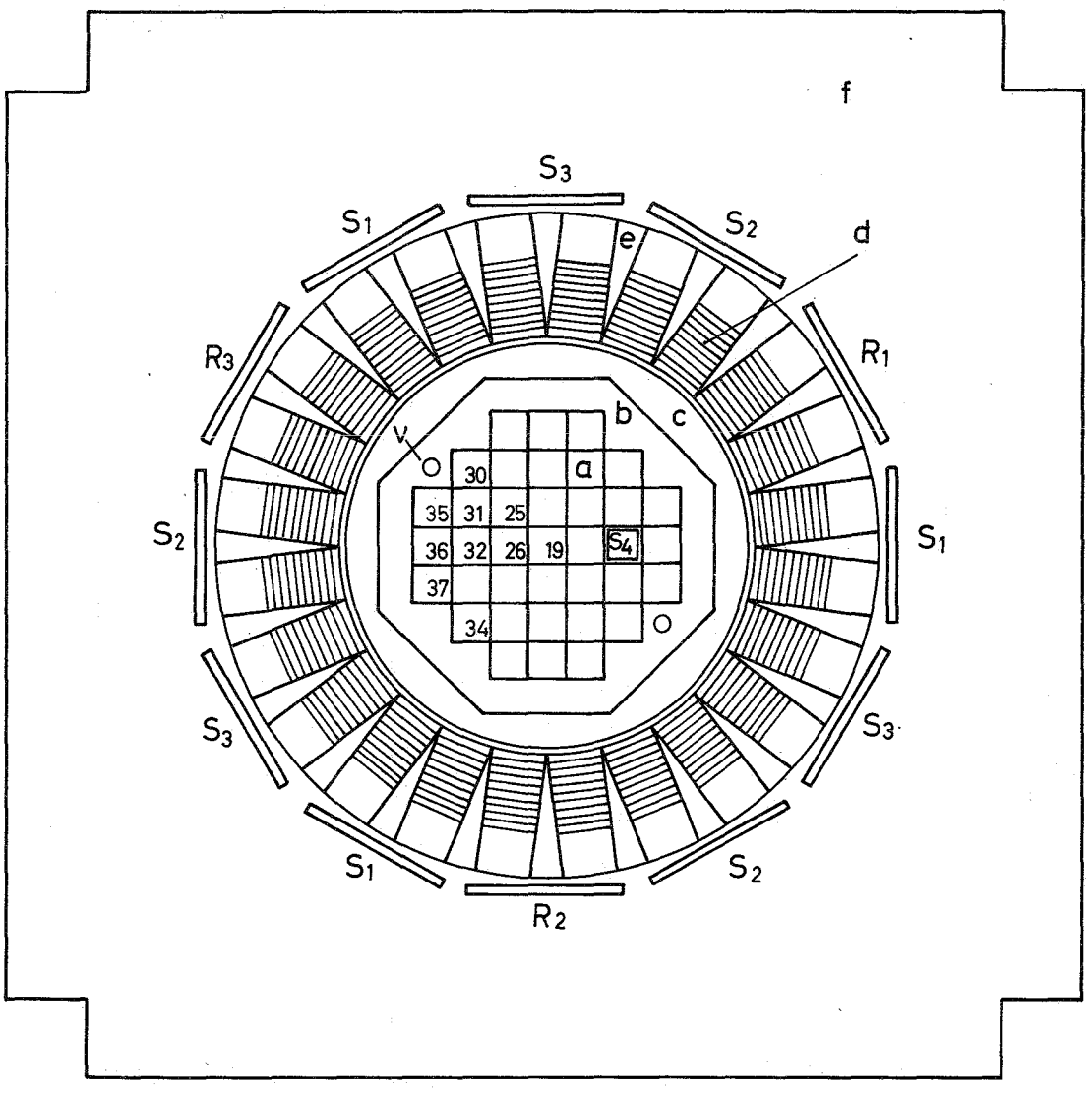

FIG.1 Schematic cross section of STARK

a - fast core
b - natural uranium zone
c - graphite region
d - thermal core (fuel region)
e - thermal core (graphite pieces)
f - graphite reflector
v - vertical channel

19; 25; 26 ... matrix positions for fission chamber and foil measurements

R_1, R_2, R_3 - fine-control plates

S_1, S_2, S_3 - safety plates

S_4 - fuel-poison safety rod

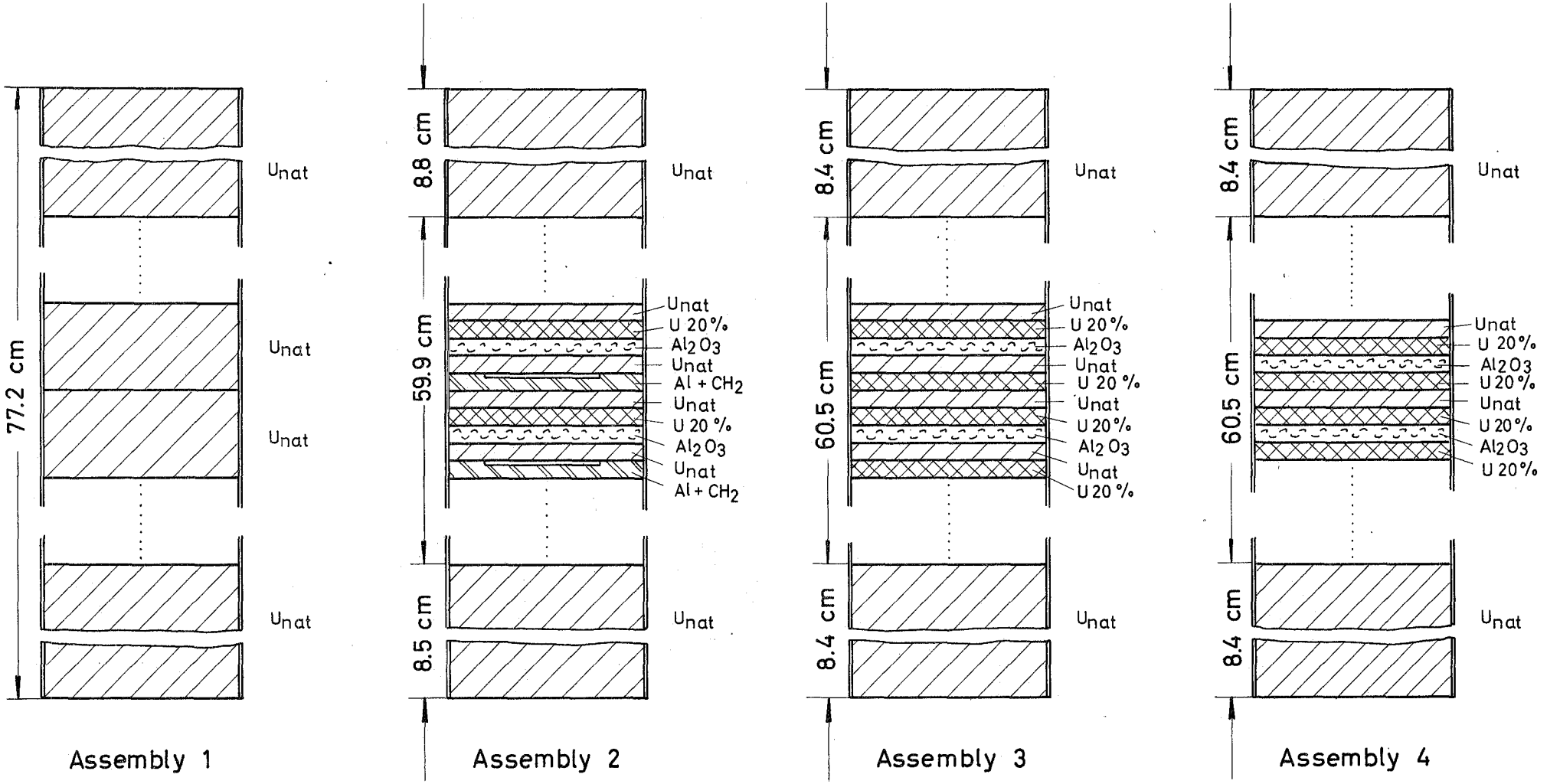

FIG.2 Loading pattern of the fast core elements

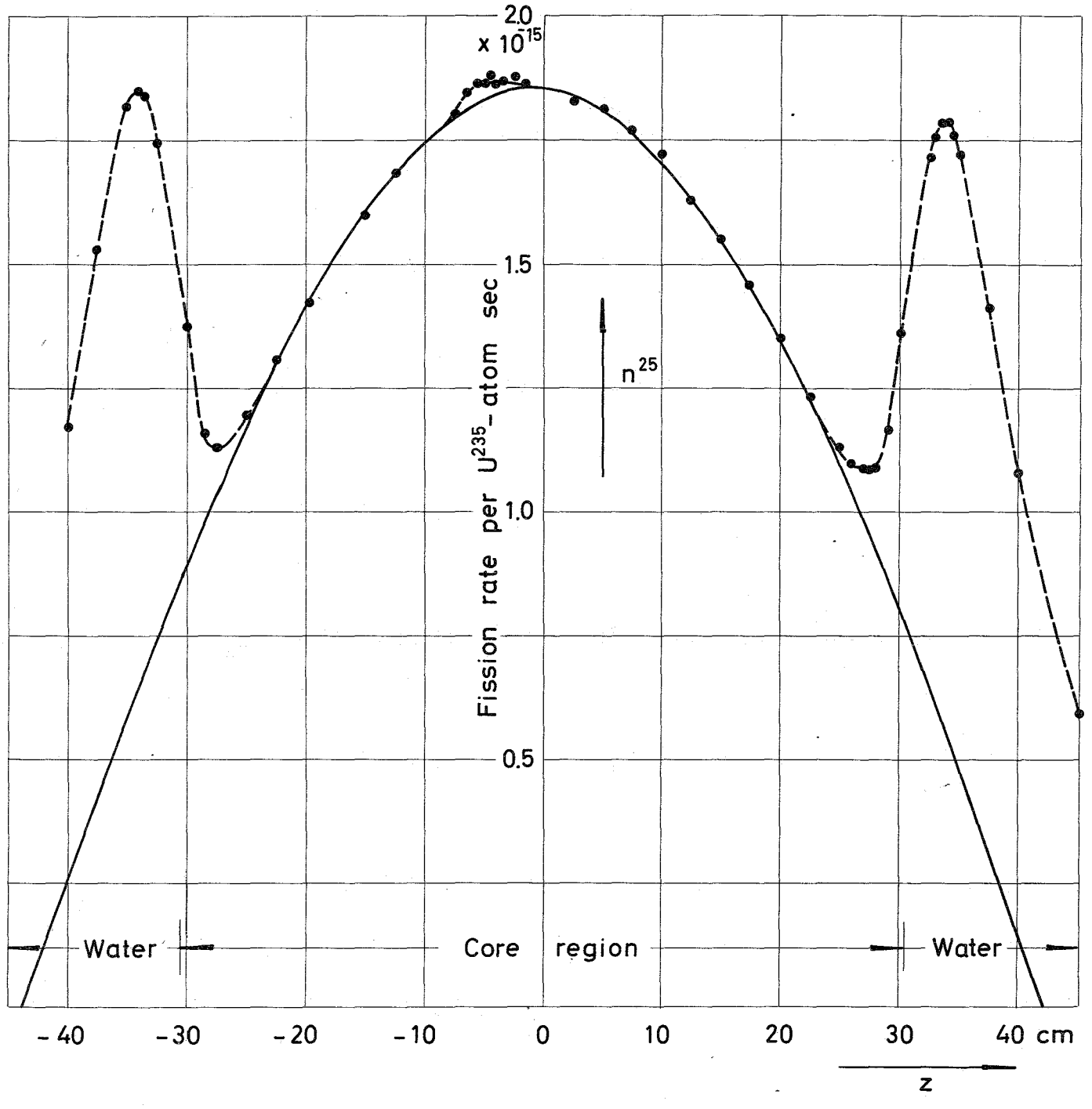

FIG.3 Axial distribution of the ^{235}U-fission rate in the thermal zone of STARK (r = 34.8 cm, Assembly 4) at 1 watt reactor power

—●—●— fission chamber traverse

——————— cos μ z-distribution

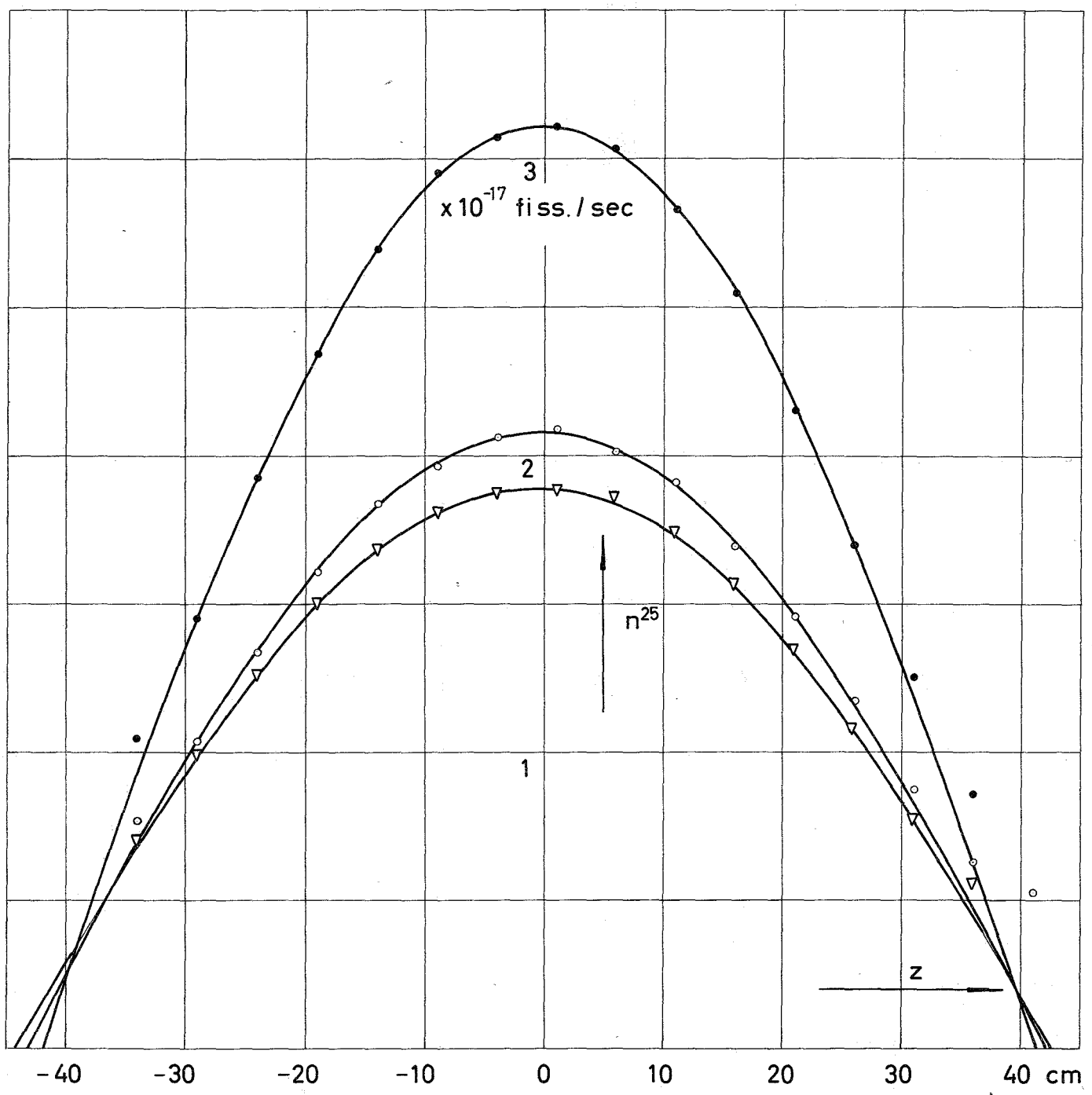

FIG.4 Axial distribution of ^{235}U-fission rate, n^{25}, per atom at ≈ 1 watt reactor power in the central matrix tube of the fast core

▽ fission chamber traverse, Assembly 2

○ fission chamber traverse, Assembly 3

• fission chamber traverse, Assembly 4

——— cos μz-distribution fitted to the experimental data

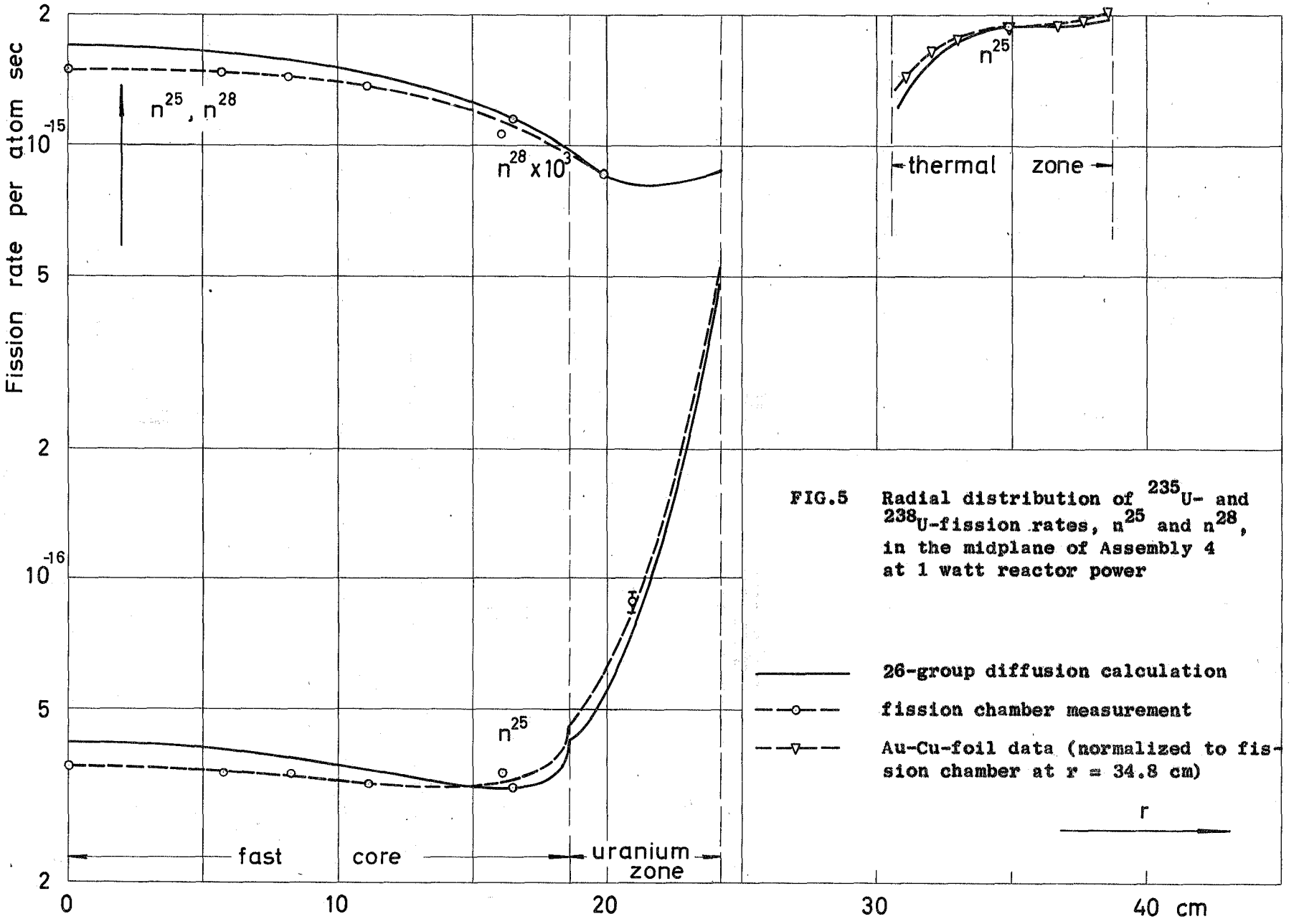

FIG.5 Radial distribution of ^{235}U- and ^{238}U-fission rates, n^{25} and n^{28}, in the midplane of Assembly 4 at 1 watt reactor power

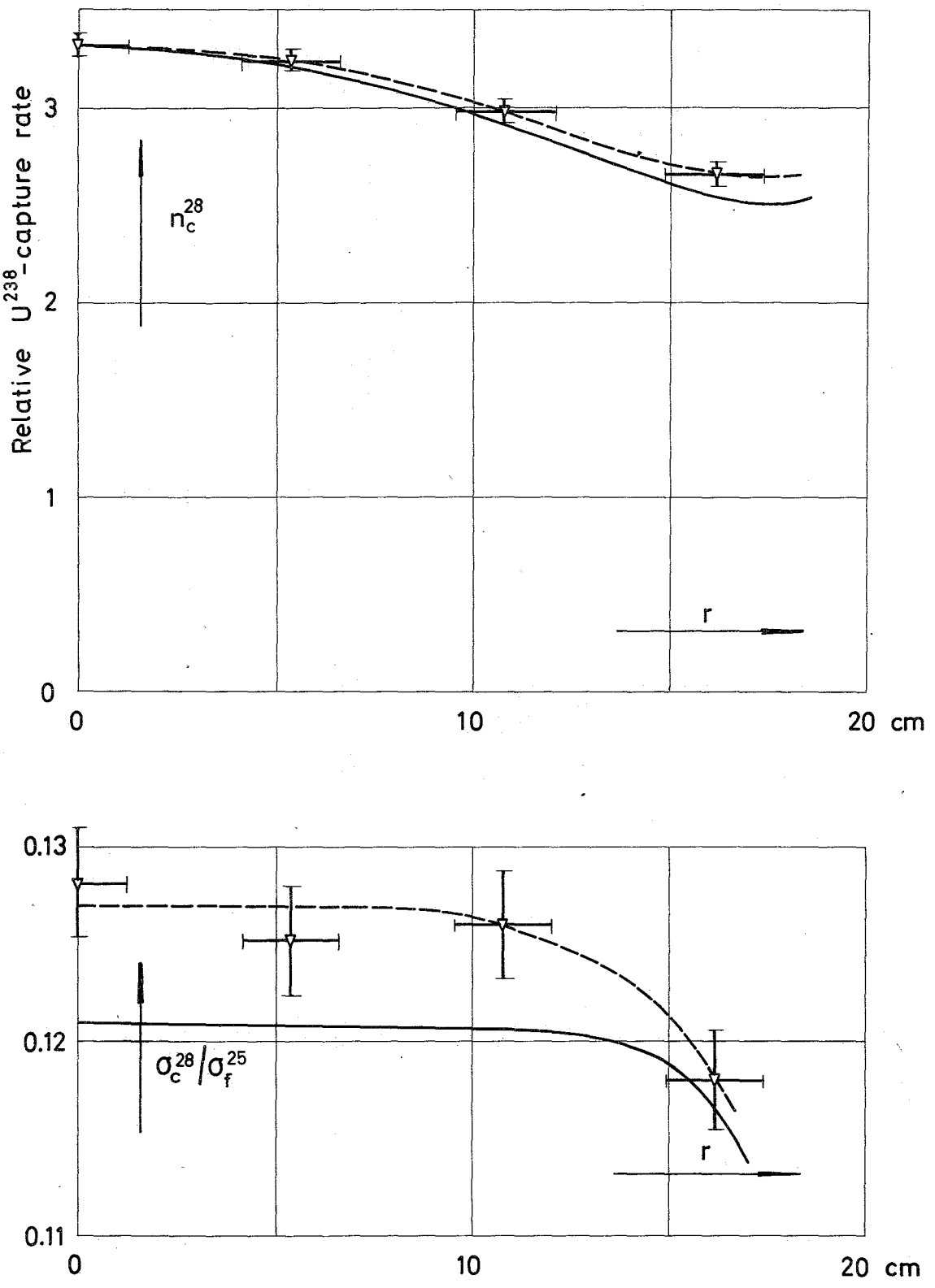

FIG.6 Radial dependence of the ^{238}U-capture rate n_c^{28} and the $^{238}U/^{235}U$-capture-to-fission ratio, $\sigma_c^{28}/\sigma_f^{25}$, in the midplane of Assembly 4

uranium foil activation

26-group diffusion calculation

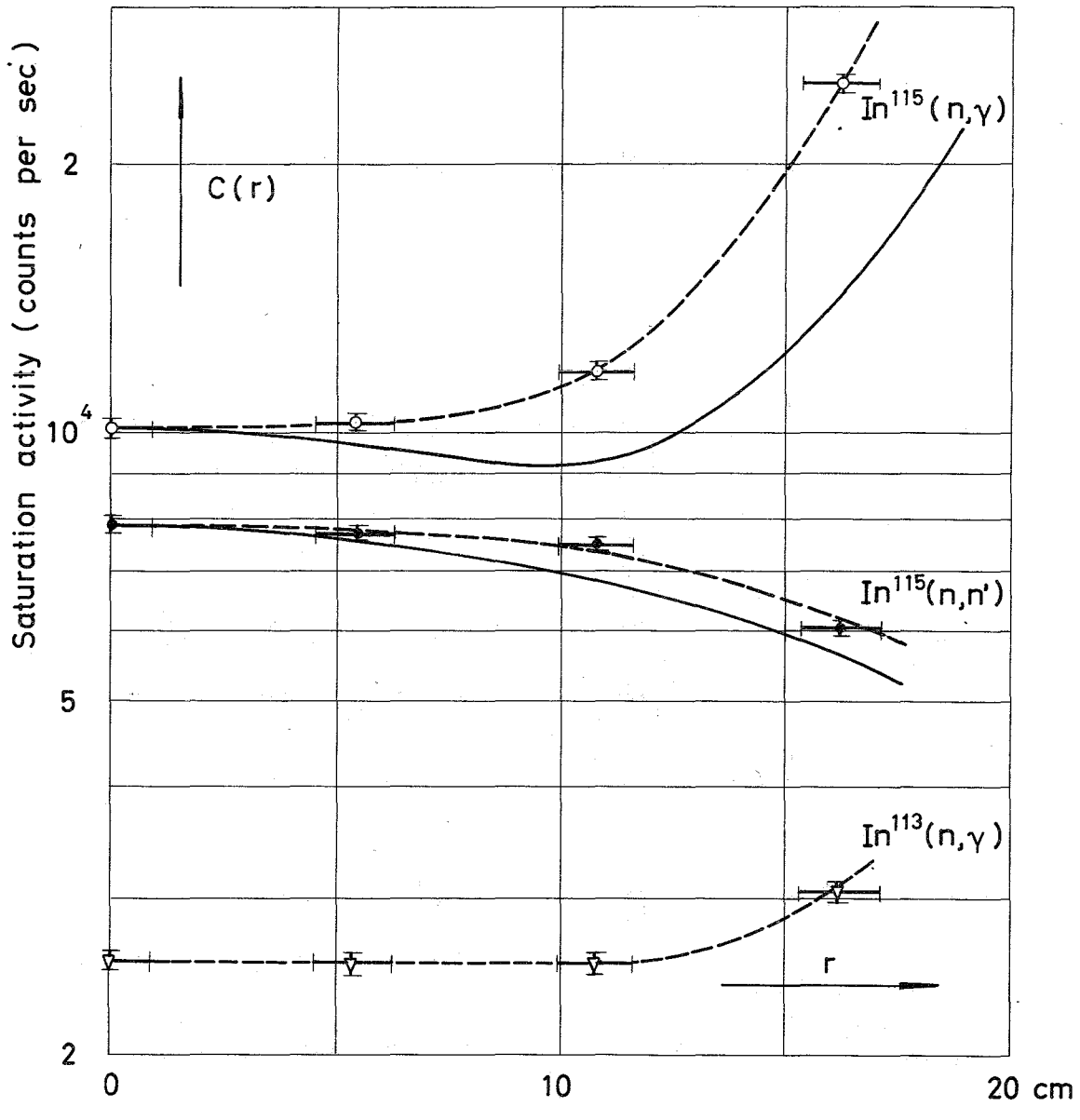

FIG.7 Radial distribution of In-foil activity C(r) in the fast zone of Assembly 4

——○—— $^{115}In(n,\gamma)^{116m}In$-reaction rate

——●—— $^{115}In(n,n')^{115m}In$-reaction rate

——▽—— $^{113}In(n,\gamma)^{114m}In$-reaction rate

———— 26-group diffusion calculation (normalized to experimental value at r = 0)

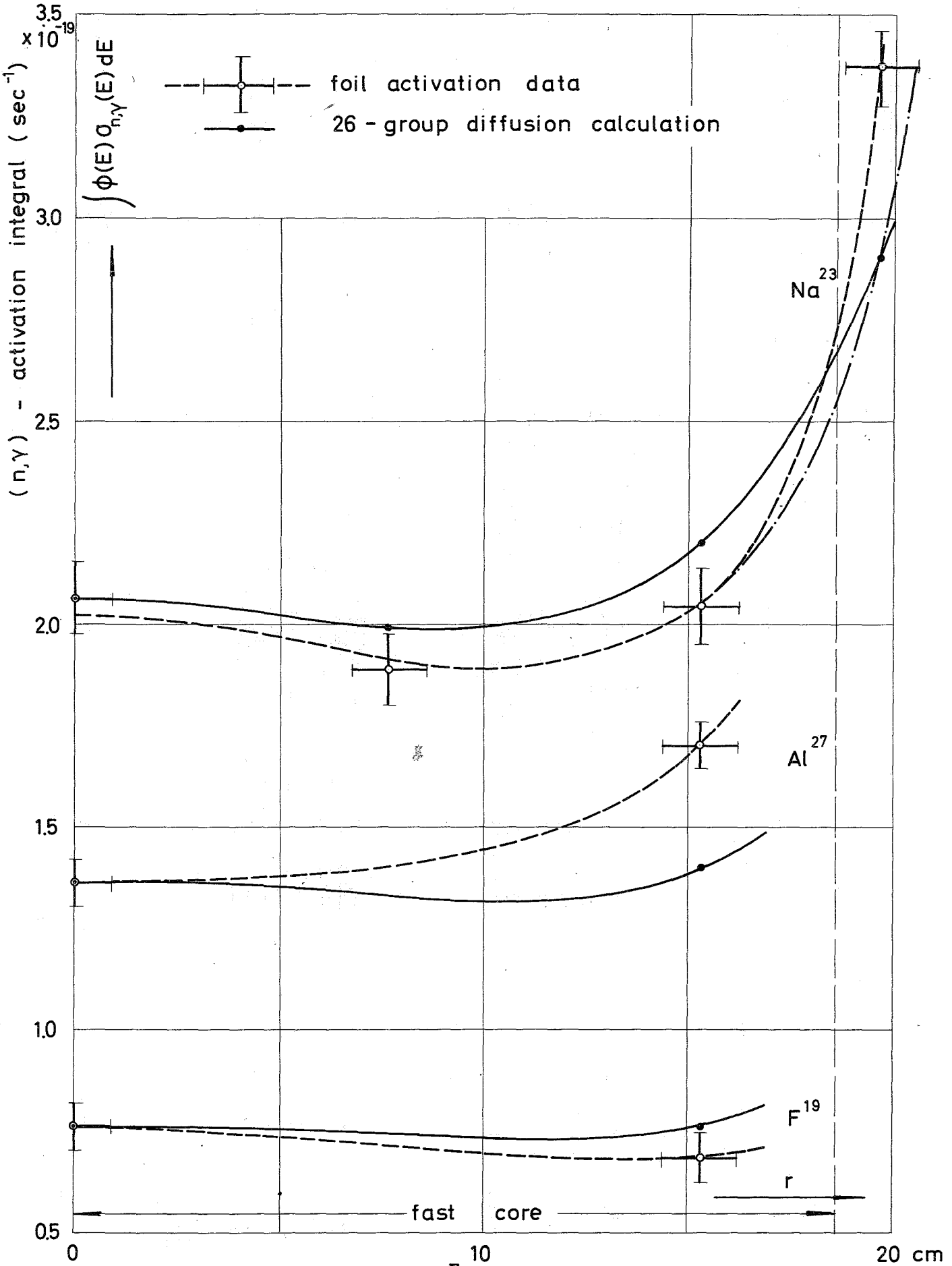

FIG.8 (n,γ)-activation integral $\int_{E_{Cd}}^{E_{fiss\ max}} \phi(E)\ \sigma_{n,\gamma}(E)\ dE$ for ^{23}Na, ^{27}Al, and ^{19}F as a function of radial position r in the midplane of Assembly 2

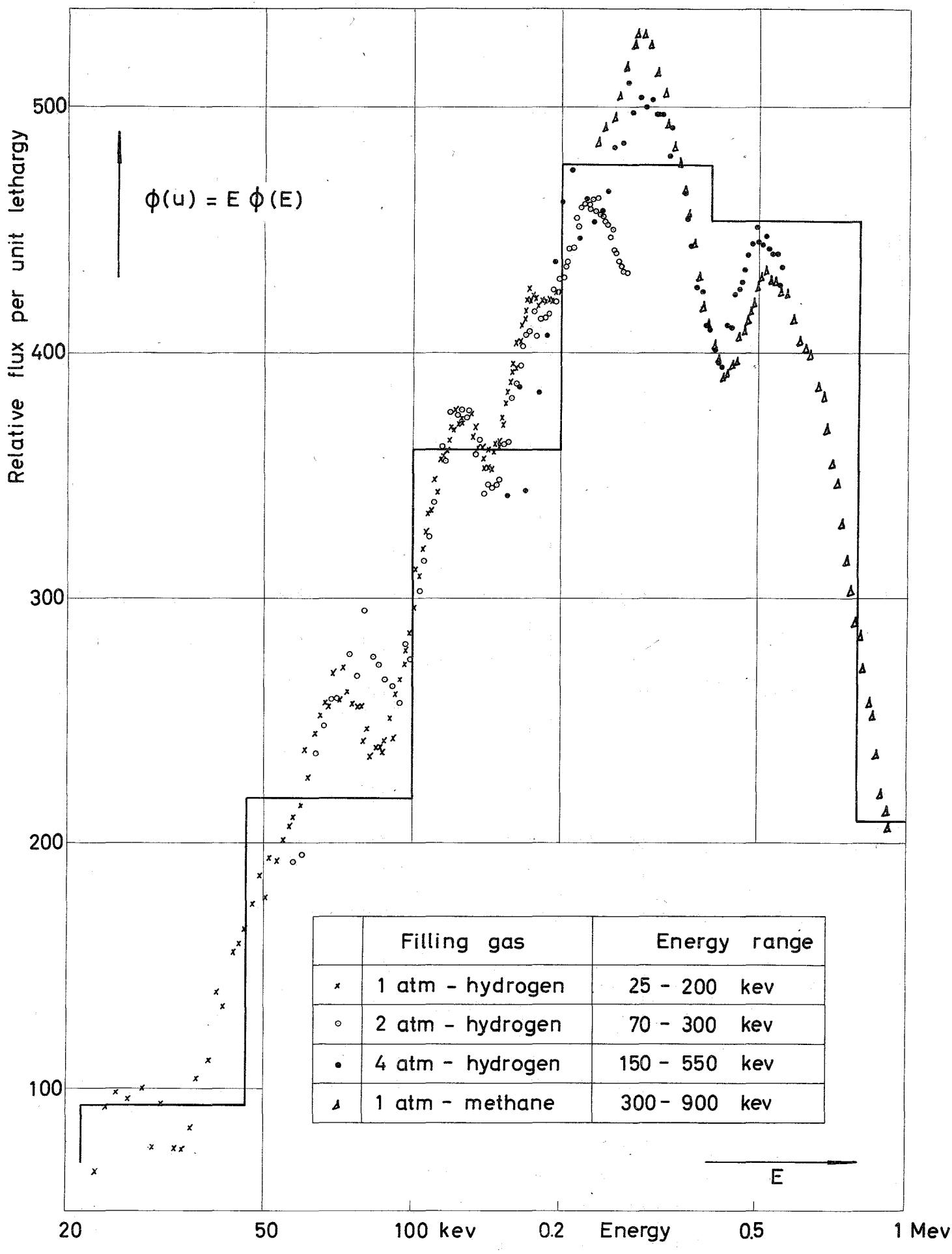

FIG.9 Neutron spectrum in the center of Assembly 4

× ○ • measurement with hydrogen-filled spherical counters

——— 26-group diffusion calculation (normalized to experiment)

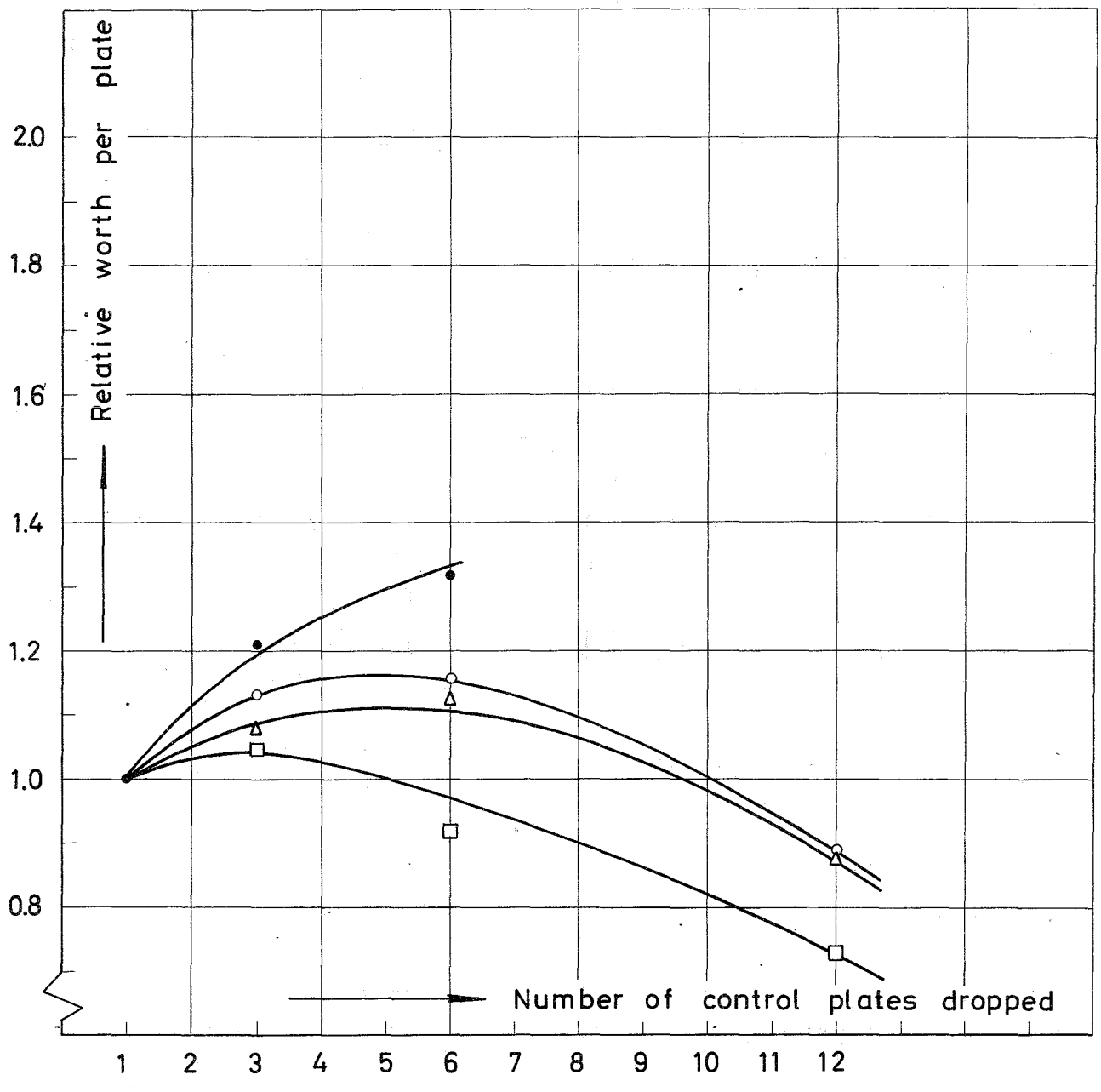

FIG.10 Reactivity worth per control plate relative to the worth of a single plate for various control plate configurations

- ● rod drop experiments, Assembly 1
- ○ rod drop experiments, Assembly 2
- △ rod drop experiments, Assembly 3
- □ rod drop experiments, Assembly 4

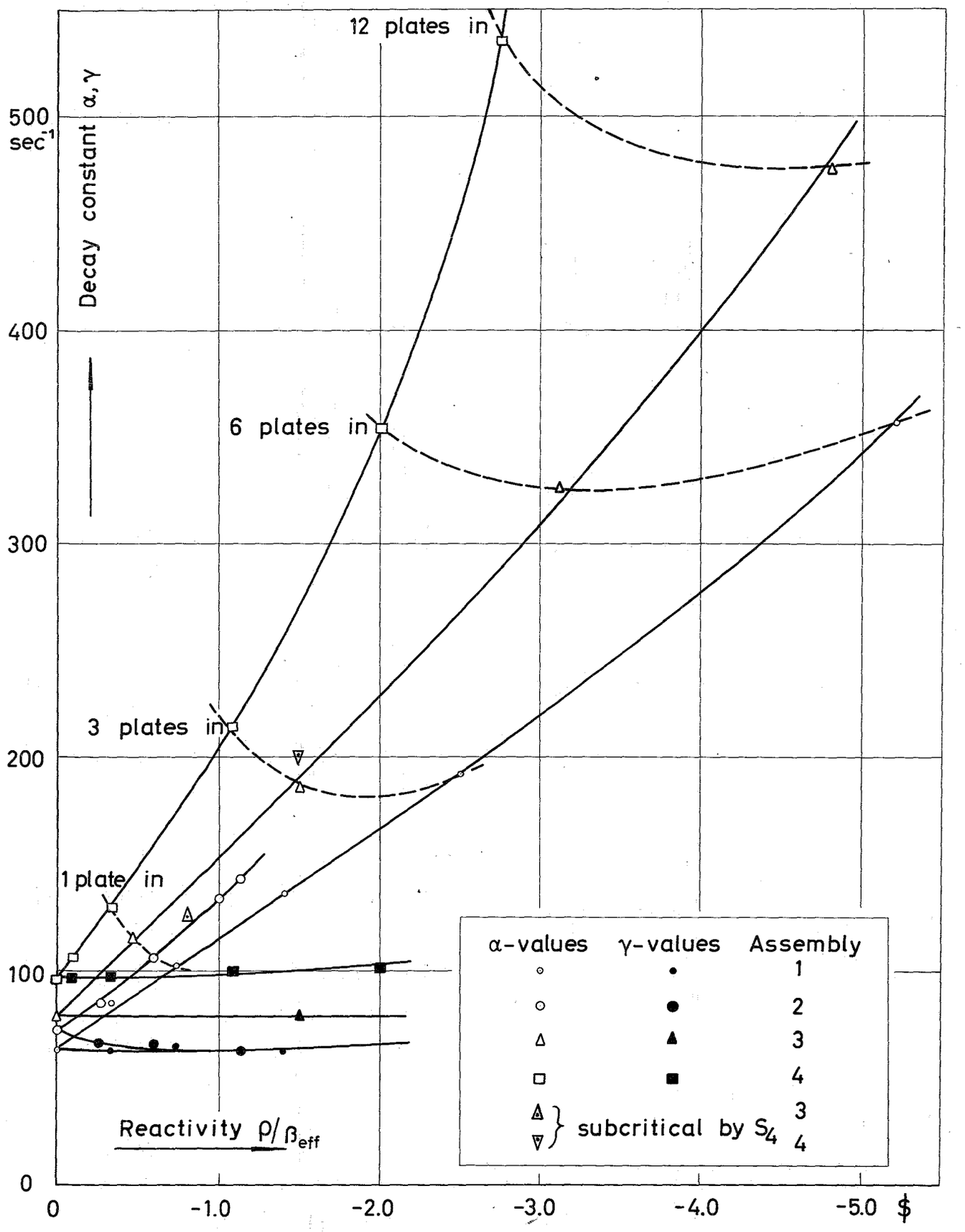

FIG.11 **Prompt-neutron decay constant α and γ = $ß_{eff}/\Lambda$ obtained by pulsed neutron experiments for different control-plate configurations vs. reactivity $\rho/ß_{eff}$ determined by rod-drop measurements**

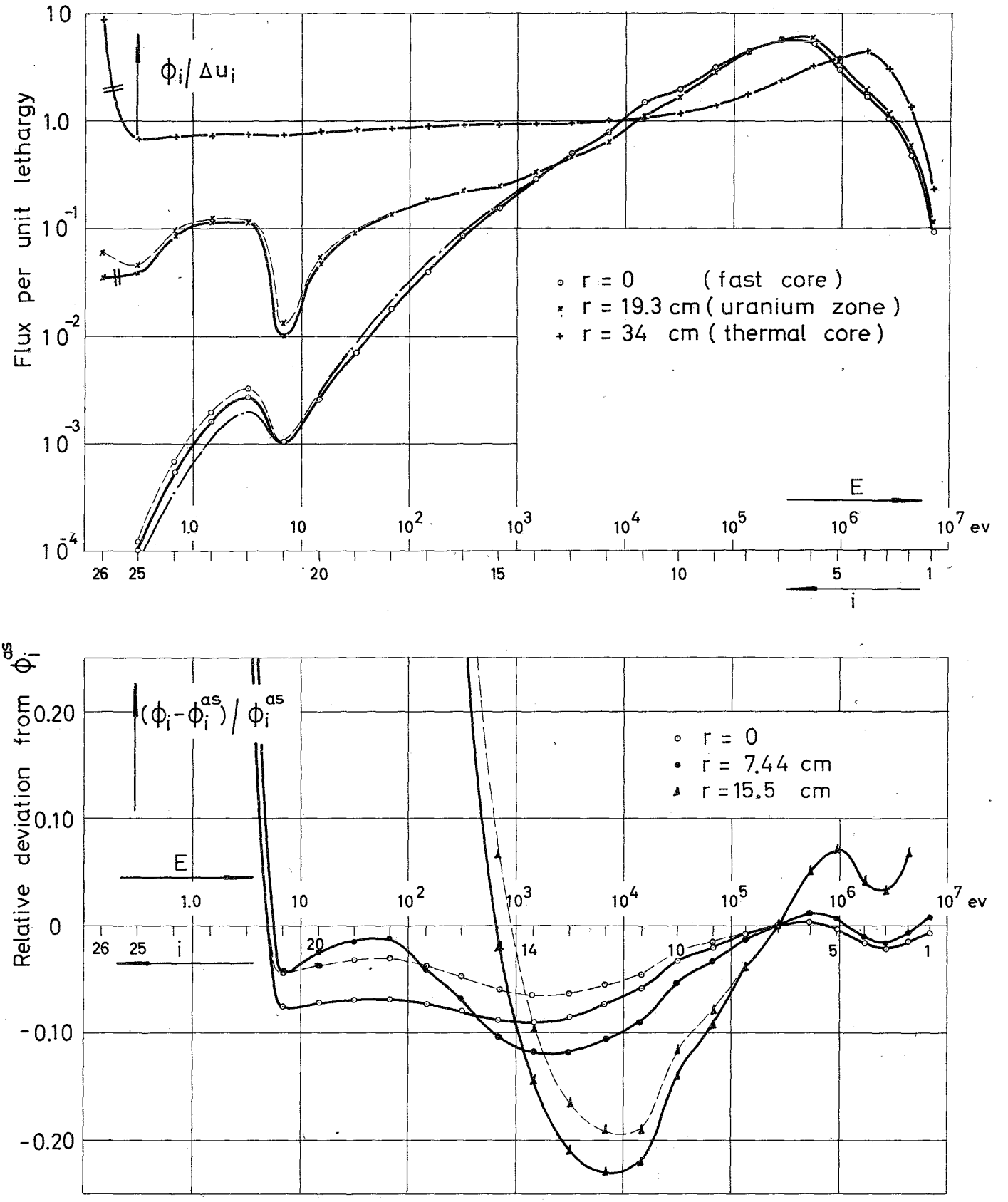

FIG.12 Neutron spectrum $\phi_i(r)$ and its deviation from the equilibrium spectrum ϕ_i^{as} at different radial positions r in Assembly 2

——— STARK spectrum, 26-group diffusion calculation

– – – – – STARK spectrum, 26-group S_4-calculation

——·—— equilibrium spectrum

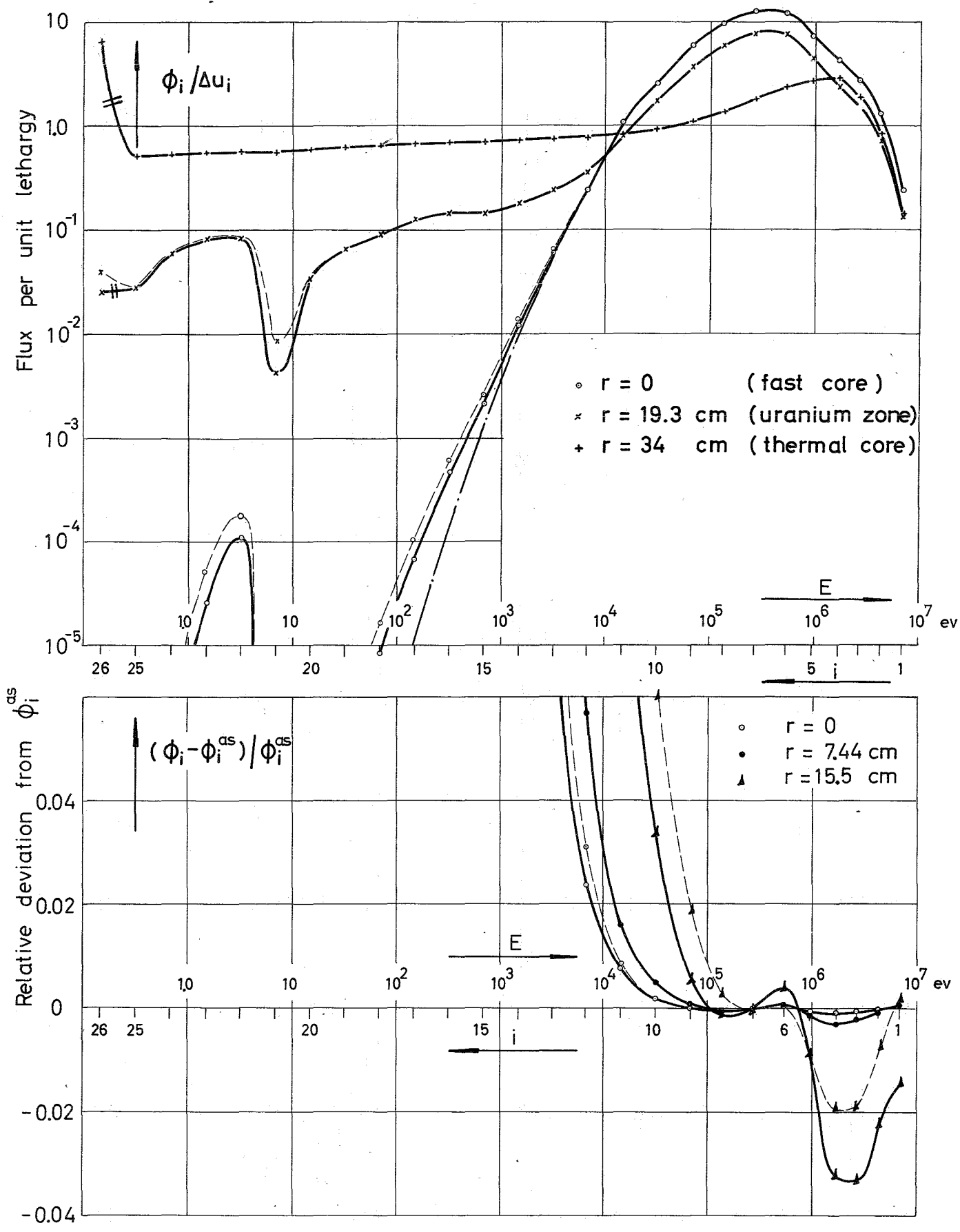

FIG.13 Neutron spectrum $\phi_i(r)$ and its deviation from the equilibrium spectrum ϕ_i^{as} at different radial positions r in Assembly 4

——— STARK spectrum, 26-group diffusion calculation

– – – – – – STARK spectrum, 26-group S_4-calculation

——·——·—— equilibrium spectrum

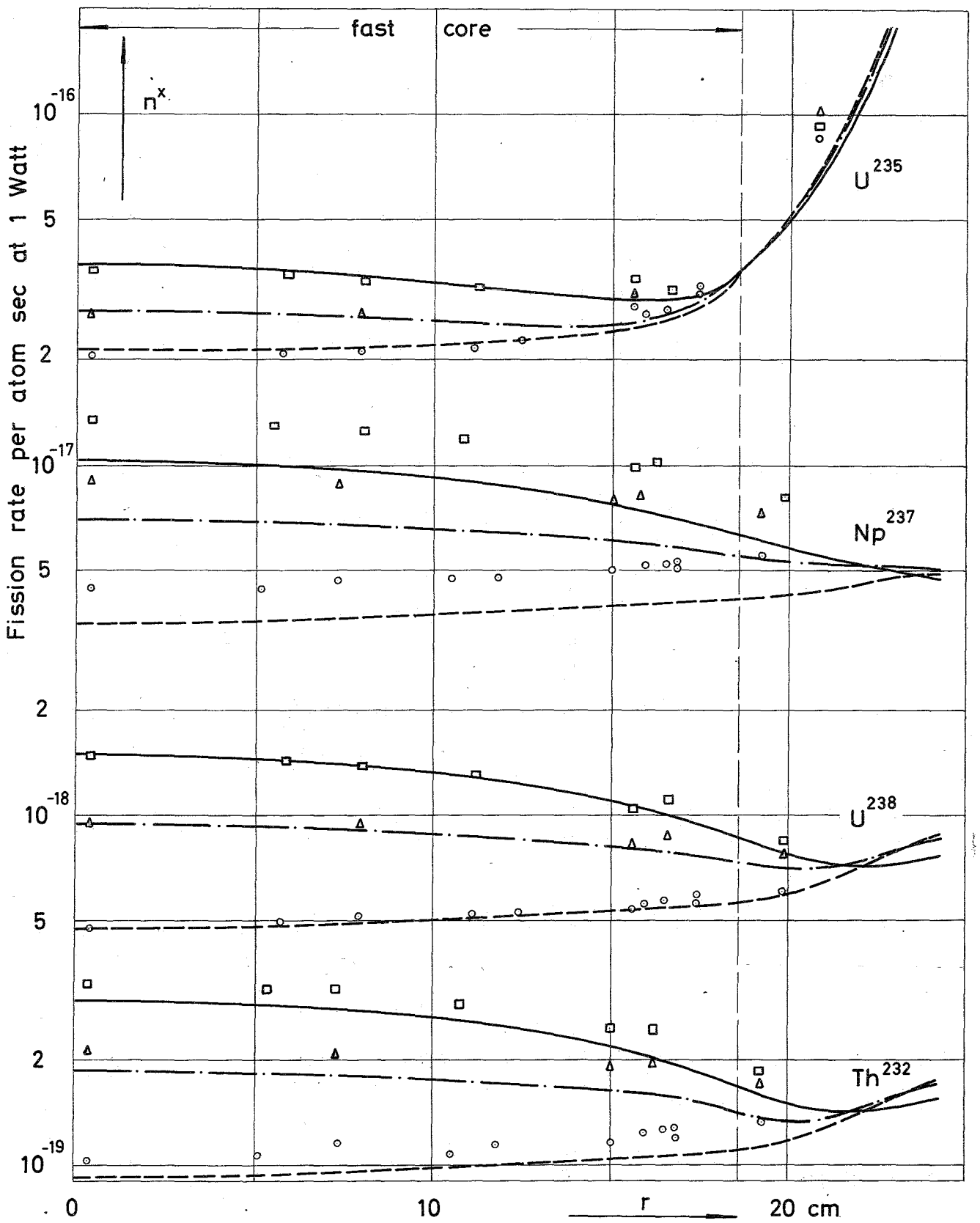

FIG.14 Radial fission rate distribution for ^{232}Th, ^{235}U, ^{238}U, and ^{237}Np obtained with cylindrical fission chambers

	exp. points	26-group diffusion calculation
Assembly 2 :	○	———
Assembly 3 :	△	——·——·
Assembly 4 :	□	———

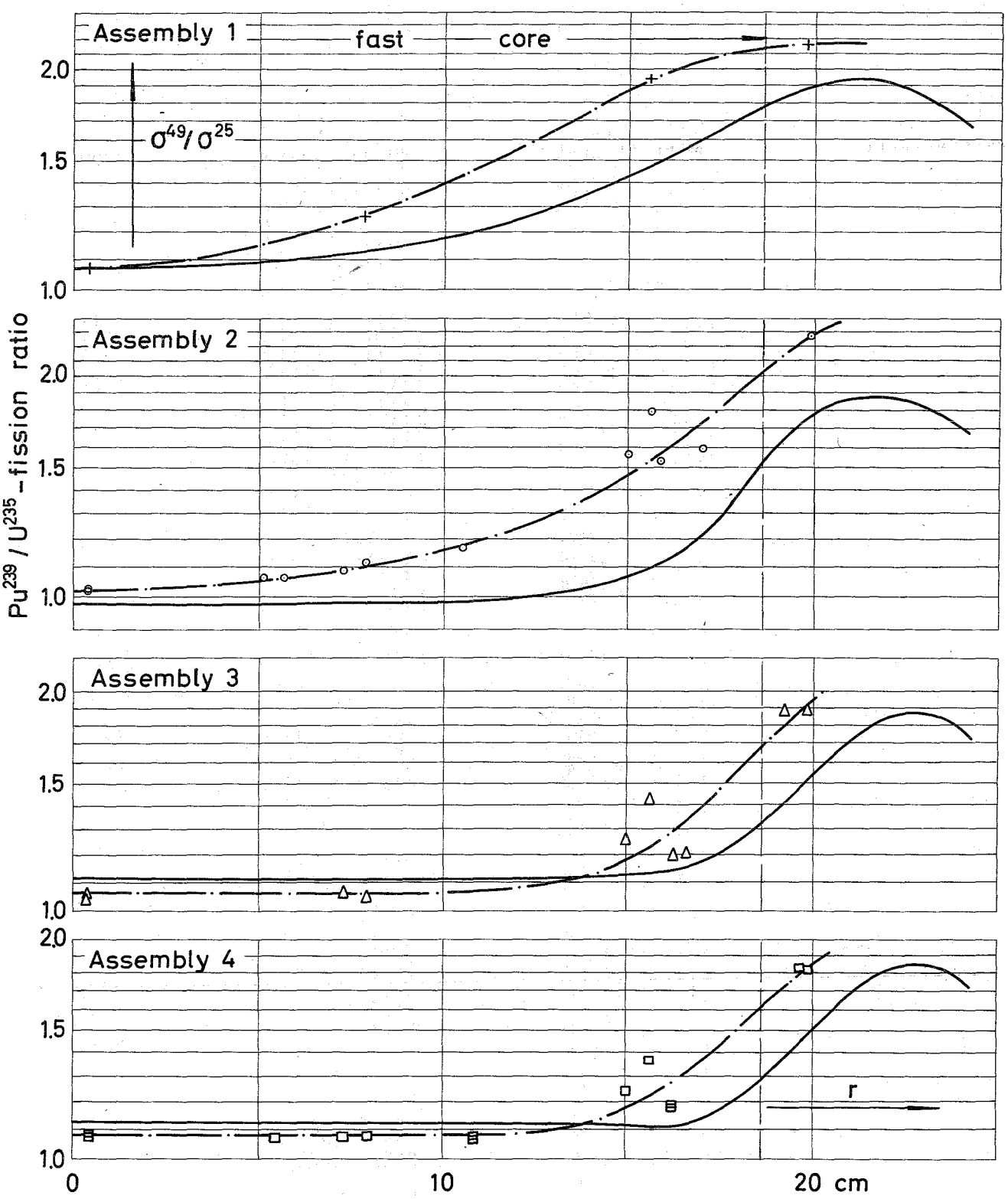

FIG.15 $^{239}Pu/^{235}U$-fission ratio in the fast zone of STARK

fission chamber data

26-group diffusion calculation

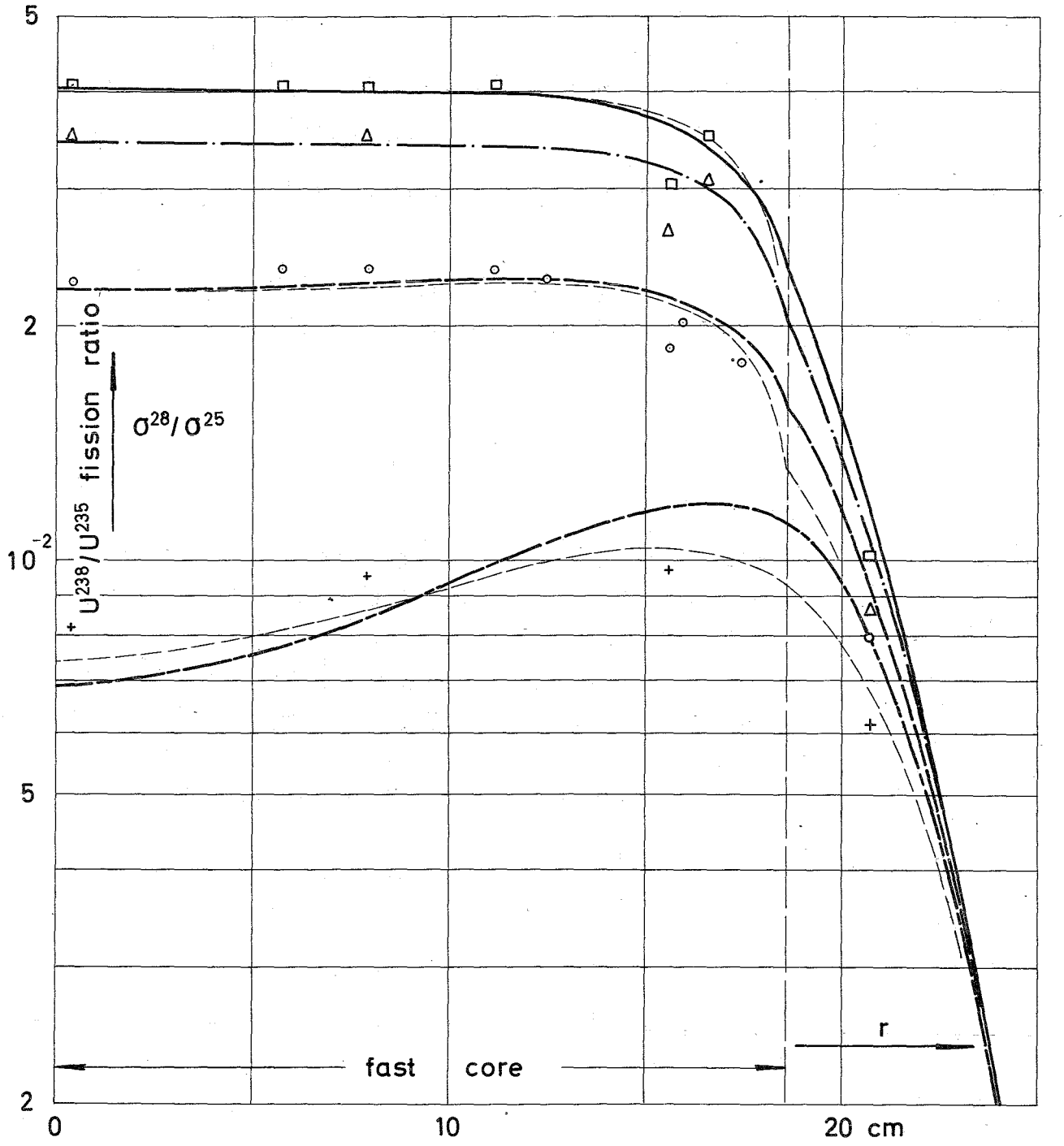

FIG.16 $^{238}U/^{235}U$-fission ratio in STARK as a function of radial position r

	exp. points	26-group diffusion calculation
Assembly 1 :	+	————
Assembly 2 :	o	————
Assembly 3 :	Δ	————
Assembly 4 :	□	————
S_4-calculation :	————	

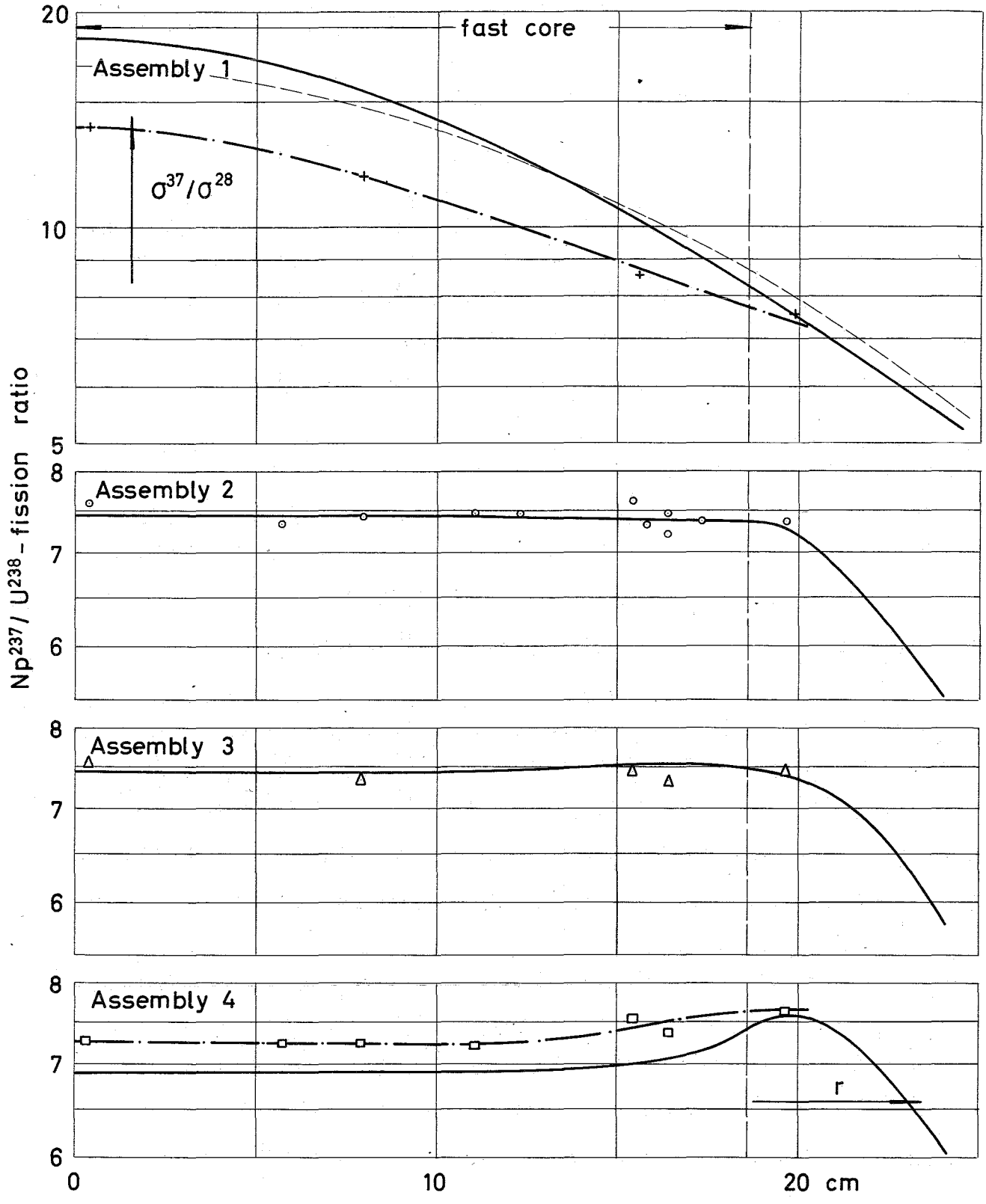

FIG.17 $^{237}Np/^{238}U$-fission ratio in the fast zone of STARK

fission chamber data

26-group diffusion calculation

26-group S_4-calculation

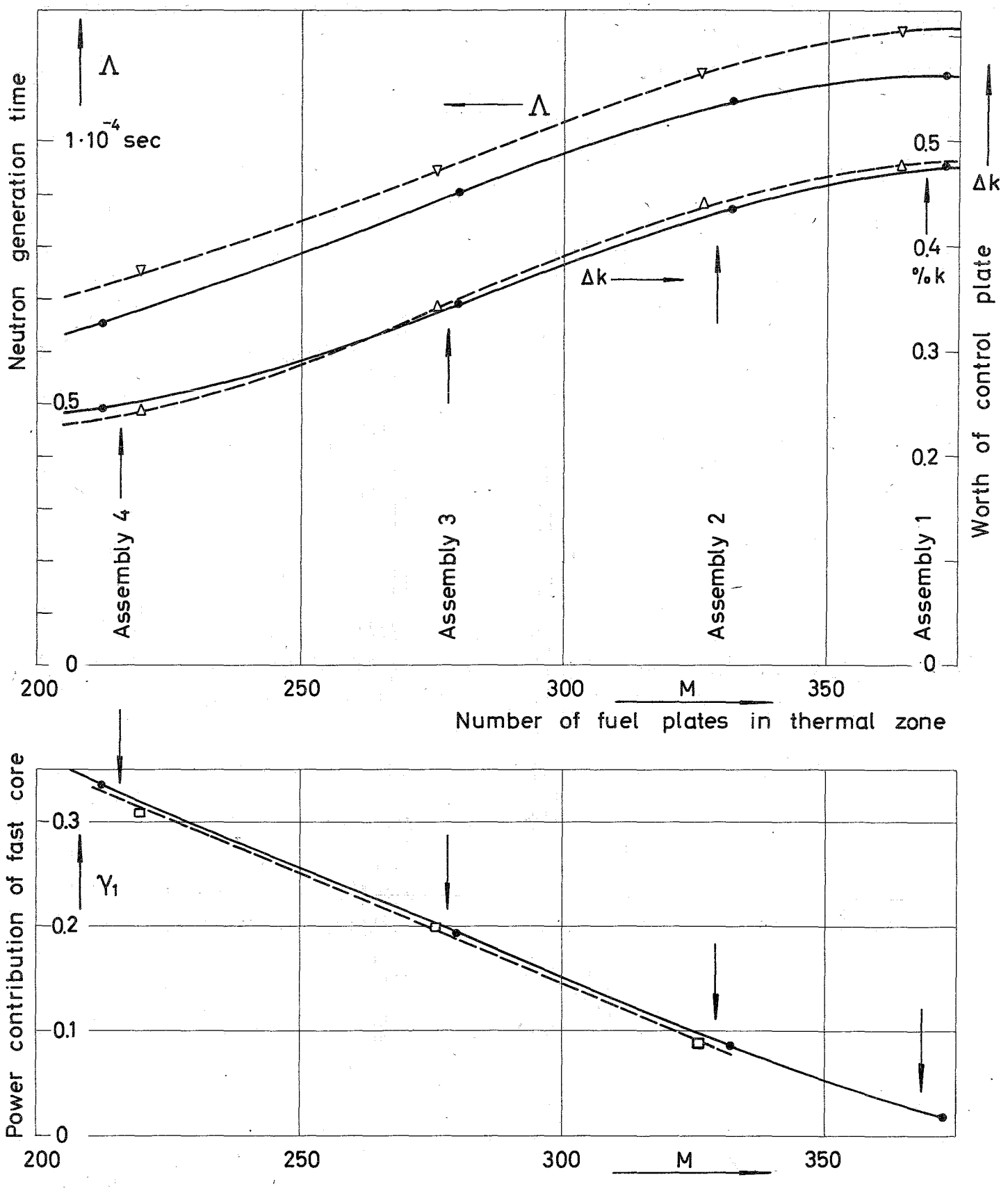

FIG.18 Variation of reactor parameters with reactor loading

—▽— generation time Λ
—△— reactivity worth Δk of one control plate } experimental
—□— power contribution γ_1 of fast zone
—●— 26-group diffusion calculation